



# RESEARCH MEMORANDUM

DOWNWASH SURVEY BEHIND TWO LOW-ASPECT-RATIO VARIABLE-  
INCIDENCE WINGS IN COMBINATION WITH THREE  
DIFFERENT SIZE FUSELAGES AT A MACH  
NUMBER OF 0.25

By Edward J. Hopkins and Norman E. Sorensen

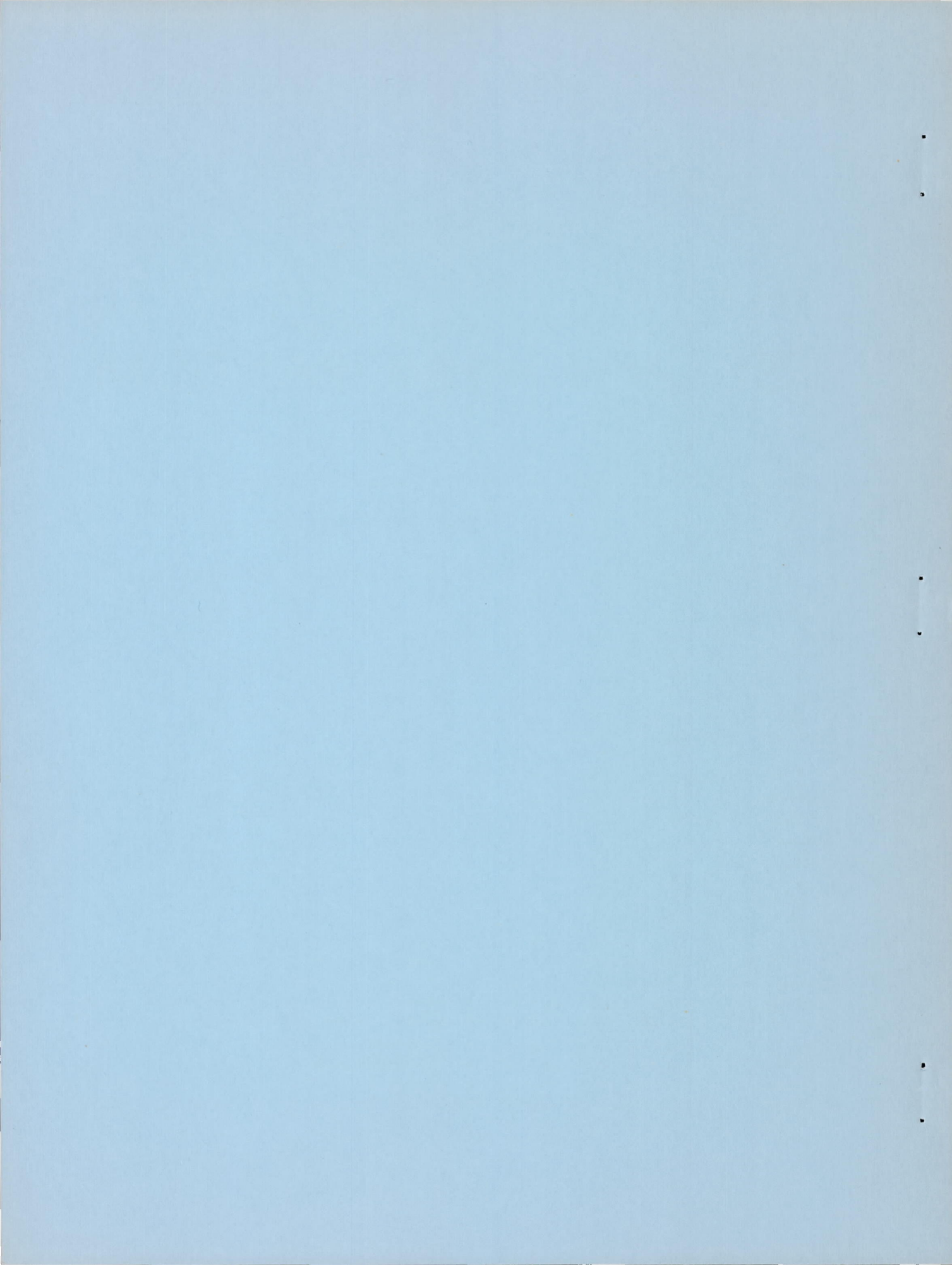
Ames Aeronautical Laboratory  
Moffett Field, Calif.

NATIONAL ADVISORY COMMITTEE  
FOR AERONAUTICS

WASHINGTON

March 30, 1955

Declassified March 26, 1956



## NATIONAL ADVISORY COMMITTEE FOR AERONAUTICS

RESEARCH MEMORANDUMDOWNWASH SURVEY BEHIND TWO LOW-ASPECT-RATIO VARIABLE-  
INCIDENCE WINGS IN COMBINATION WITH THREE  
DIFFERENT SIZE FUSELAGES AT A MACH  
NUMBER OF 0.25

By Edward J. Hopkins and Norman E. Sorensen

## SUMMARY

A wind-tunnel investigation has been conducted to determine the downwash angles in a transverse plane behind the wings of six wing-body combinations at a Mach number of 0.25. A triangular wing having an aspect ratio of 2.0 and a trapezoidal wing having an aspect ratio of 3.0 were tested in combination with three geometrically similar slender bodies of revolution. For each wing, the ratios of maximum body diameter to wing span were 0.196, 0.259, and 0.343. A range of angles of attack from 0° to 20° was covered at angles of wing incidence ranging from 0° to 10° for each wing-body combination.

The measured downwash angles at small angles of attack and at a wing incidence of 0° are compared with those predicted by a numerical method in which no account was taken of the distortion or roll-up of the vortex sheet.

## INTRODUCTION

In a previous experimental investigation, a study was made of the mutual interaction of the wing and the body on the aerodynamic forces and moments for several wing-body combinations having variable-incidence wings. As part of a general study of these wing-body combinations employing low-aspect-ratio wings and relatively large bodies, the present investigation was undertaken to measure the downwash in a plane behind six wing-body combinations reported upon in references 1 and 2. This downwash survey was made throughout an angle-of-attack range from 0° to 20° with the wings at angles of incidence ranging from 0° to 10°.

A limited theoretical analysis involving a numerical solution for an array of discrete line vortices is also presented for small angles of attack at a wing incidence of  $0^\circ$ . In this analysis, which is similar to that used in reference 3, the displacement and roll-up of the vortex sheet were not taken into account because of insufficient knowledge of the span loading and flow separation from the wings at the high angles of attack. The authors wish to acknowledge the helpful suggestions and assistance of Mr. Stewart M. Crandall of Ames Aeronautical Laboratory in making the numerical calculations.

## NOTATION

b wing span

c local wing chord

$\bar{c}$  mean aerodynamic chord, 
$$\frac{\int_{-b/2}^{b/2} c^2 dy}{\int_{-b/2}^{b/2} c dy}$$

$c_L$  lift coefficient,  $\frac{\text{lift}}{qS}$

$c_N$  normal-force coefficient,  $\frac{\text{normal force on exposed wing panel}}{qS}$

d maximum body diameter

$\frac{d}{b}$  ratio of maximum body diameter to wing span

$i_w$  angle of wing incidence relative to the body axis (positive with wing trailing edge down)

L body length

r body radius

$r_o$  maximum body radius

S total wing area

q	free-stream dynamic pressure
x	distance along the body axis from the nose of the body
y	lateral distance from the vertical plane of symmetry
$\frac{y}{b/2}$	lateral distance in wing semispans from the vertical plane of symmetry
$\frac{z}{b/2}$	distance in wing semispans perpendicular to the plane of the wing ( $i_w = 0^\circ$ )
$\alpha$	body angle of attack
$\alpha_{C_N \max}$	angle of attack above which the normal force on the exposed wing panel first begins to decrease with an increase in angle of attack (See sketch in "RESULTS AND DISCUSSION" section.)
$\epsilon$	angle of downwash in the plane of the survey rake
$\psi$	angle of yaw

#### MODEL AND APPARATUS

Three geometrically similar bodies were combined alternately with a wing having a triangular plan form and with a wing having a trapezoidal plan form. The bodies are shown with their equation in figure 1(a) and are described in reference 1. Each wing had the same span which resulted in ratios of maximum body diameter to wing span of 0.196, 0.259, and 0.343. The wings were mounted on the bodies in the positions shown in figure 1. The angle of wing incidence was varied by rotating the wing panels about a lateral axis which passed through the mid-point of the wing root chord.

The triangular wing had an aspect ratio of 2.0, a taper ratio of 0, and a leading-edge sweepback of  $63.43^\circ$ . This wing had an NACA 0005 section (modified as shown in fig. 1(b)) in vertical planes parallel to the wing root chord. The trapezoidal wing had an aspect ratio of 3.0, a taper ratio of 0.4, and a leading-edge sweepback of  $23.17^\circ$ . This wing had a hexagonal section 4.5-percent-chord thick with rounded ridge lines as shown in figure 1(c).

Downwash measurements were made by means of the rake of transverse tubes which was attached to and moved with the body (see figs. 2 and 3). It was mounted in a plane normal to the body axis at the position shown in figure 1. The tubes of the rake were made of highly polished stainless steel (3/4-inch outside diameter, 1/16-inch wall). The bottom tube was not used because of its proximity to the wind-tunnel floor at the high angles of attack.

## TEST PROCEDURE

Tests were conducted in one of the Ames 7- by 10-foot wind tunnels at a dynamic pressure of 90 pounds per square foot. The Mach number was approximately 0.25 and the Reynolds numbers (based on the mean aerodynamic chords) were approximately 4 and 2 million for the triangular and trapezoidal wings, respectively. Measurements were made of the downwash fields of all the wing-body combinations for each angle of wing incidence ( $0^\circ$ ,  $2^\circ$ ,  $4^\circ$ ,  $6^\circ$ ,  $8^\circ$ , and  $10^\circ$ ) through an angle-of-attack range from  $0^\circ$  to  $20^\circ$ .

The survey rake was calibrated in the wind tunnel at a dynamic pressure of 90 pounds per square foot through a wide range of downwash angles. A preliminary calibration of a representative single-tube rake indicated that the downwash-angle calibrations would be influenced less than 1 percent by yawed flow ( $\psi = 0^\circ$  to  $60^\circ$ ) or by dynamic-pressure changes ( $q = 30$  to 90 lb/sq ft).

## CORRECTIONS AND ACCURACY

Corrections for the effects of the wind-tunnel walls were applied to the angles of attack by the method of reference 4. These corrections are as follows:

$$\alpha = \alpha_u + 0.77 C_{Lu} \quad (\text{triangular wing})$$

$$\alpha = \alpha_u + 0.38 C_{Lu} \quad (\text{trapezoidal wing})$$

where the subscript  $u$  denotes the uncorrected values. Values of  $C_{Lu}$  were obtained from the experimental data in references 1 and 2. At a given uncorrected angle of attack, the same corrections were assumed and applied to each angle of downwash as were applied to the angle of attack. This procedure approximately corrects each angle of downwash for the influence of the wind-tunnel walls on the trailing vortices, but neglects the correction for the influence of the wind-tunnel walls on the bound vortex. It was estimated from reference 5 that the correction for the bound vortex would increase the downwash-curve slope,  $d\epsilon/d\alpha$ , by only 0.015. It was also estimated that additional corrections to the angles of downwash for the survey positions being off the center line of the wind tunnel would increase the above correction by not over 10 percent.

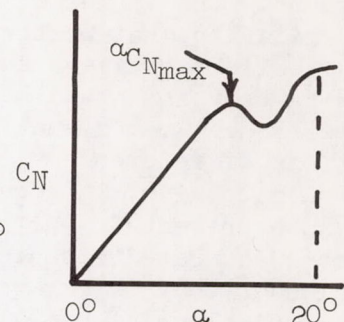
To indicate the accuracy of the measurements of the downwash made by the transverse-tube rake, a limited survey was made with a conventional single-tube directional pitot. Measurements were made at the same stations as those by the transverse-tube rake behind the wing-body combination having the trapezoidal wing and a maximum body diameter-to-span ratio of 0.196. Agreement between the downwash slopes,  $d\epsilon/d\alpha$ , for the two sets of data was within the experimental accuracy.

## RESULTS AND DISCUSSION

Downwash angles are presented as a function of angle of attack at given distances normal to the wing plane ( $i_w = 0^\circ$ ) for each wing-body combination at a constant angle of wing incidence. For the combinations having the trapezoidal wing the angle-of-attack range covered,  $0^\circ$  to  $20^\circ$ , is beyond the angle of attack  $\alpha_{C_{N\max}}$  as shown in the sketch. The values

of  $\alpha_{C_{N\max}}$  from reference 1 are presented in

figure 4 for the three wing-body combinations having the trapezoidal wing. As indicated in reference 2, the combinations having the triangular wing reached their maximum normal-force coefficients at angles of attack above  $20^\circ$ . The downwash results are presented for all the wing-body combinations in figures 5 to 10. An index to the downwash data is presented in table I.



At low angles of attack for a wing incidence of  $0^\circ$ , the values of  $d\epsilon/d\alpha$  were generally smaller below the plane of the wing than at corresponding distances above this plane for all the wing-body combinations (e.g., figs. 5(a) and 8(a)). This result may be attributed primarily to the vertical displacement of the trailing vortex sheet. At higher angles of attack the change in sign of  $d\epsilon/d\alpha$  at 0.12 and 0.35 wing semispans above the wing plane indicates an inward lateral movement of the concentrated vortex regions. Furthermore, as the angle of attack increased, the sign change in  $d\epsilon/d\alpha$  occurred progressively closer to the vertical plane of symmetry for both wings (e.g., figs. 5(a) and 8(a)). The approximate distance behind the trailing edge of the wing for the roll-up process to be complete is given in reference 6 for an elliptic span loading as  $0.56 A/C_L$  semispans, where  $A$  is the aspect ratio. From this expression it can be estimated that for a given angle of attack the trailing vortex sheets from the triangular and from the trapezoidal wings of this investigation should roll up at approximately the same rate since the spans and ratios of aspect ratio to lift coefficient are approximately the same for both wings.<sup>1</sup> However, the distance from the survey plane to the trailing edge of the trapezoidal wing was about twice that for the triangular wing. At the survey plane the roll-up process should be more complete, therefore, for the trapezoidal wing than for the triangular wing. This prediction is substantiated by experiment as shown by comparing figure 5(a) with figure 8(a) at 0.12 semispans above the wing plane. The sign change in  $d\epsilon/d\alpha$  occurs at lower angles of attack and for a given angle of attack closer to the body for the trapezoidal wing than for the triangular wing.

<sup>1</sup>For example, with the smallest diameter-to-span ratio of 0.196, the results of references 1 and 2 indicate that the ratios of aspect ratio to lift-curve slope are 50 and 48 for the combinations having triangular and trapezoidal wings, respectively.

The values of  $d\epsilon/da$  were predicted for each wing-body combination with an angle of wing incidence of  $0^\circ$ . No attempt was made to calculate  $d\epsilon/da$  at high angles of attack because of the flow separation at the tips of the wings tested. This flow separation would, of course, affect the spanwise distribution of the load and the circulation. With the calculations restricted to small angles of attack, it was not necessary to include the effects of roll-up or distortion of the vortex sheet in the calculations. The values of  $d\epsilon/da$  were calculated herein by a numerical method similar to that presented in reference 3 in which an array of doubly infinite line vortices, extending from plus to minus infinity, replaced each wing-body combination. This method was shown to give reliable results in reference 3. An analytical solution, based on the slender-body considerations of reference 7, was checked at several survey positions and was found to give, in general, downwash-curve slopes slightly higher than those presented. With the downwash from slender-body theory corrected for more accurate values of lift-curve slope, the values of  $d\epsilon/da$  from slender-body theory would have been in close agreement with those from the numerical solution. In the vortex system used, the wing was replaced by 20 line vortices of equal strength (10 on each side of the body between the body surface and the wing tip), and the body was replaced by image vortices of each of the wing vortices. The lateral spacing of the wing vortices was governed by the elliptical distribution of load which was assumed on the exposed wing panels. An elliptic span load distribution very closely approximates the theoretical loading for each wing-body combination. (See fig. 6 of ref. 1.) The procedure followed in spacing these wing vortices was the same as that presented in reference 3. At a given angle of attack, the strengths of these wing vortices were derived from the predicted values of the normal force for the wings in the presence of the bodies as given in references 1 and 2. The vortices within the bodies were of such strengths and were so positioned that the boundary condition of no flow through a cylindrical body was satisfied. All the vortices were assumed to remain in the plane of the wing at a given small angle of attack. The equations which were used in the calculations are given in Appendix A.

The predicted results are presented for each survey position for the wing-body combinations having the triangular wing in figures 5(a), 6(a), and 7(a) and for the wing-body combinations having the trapezoidal wing in figures 8(a), 9(a), and 10(a). Except for the survey positions in the wing plane and close to the body, the theory generally gives a good estimate of  $d\epsilon/da$  at small angles of attack. In the wing plane the experimental values of  $d\epsilon/da$  differ markedly from the theoretical values, probably because of the influence of wing wake (e.g., figs. 5(a) and 8(a)).

## APPENDIX A

The procedure used in predicting the downwash angles presented herein was similar to that of reference 3 and is as follows:

1. The downwash contributed by the wing,  $w_w$ , was computed from an array of doubly infinite line vortices (10 on each side of the body) which replaced the wing. These vortices were in the extended wing-chord plane since no roll-up of the vortex sheet was assumed. The wing downwash velocities were computed from the Biot-Savart equation as:

$$(w_w)_i = \frac{\Gamma_{\max}}{\pi b} \sum_{j=1}^n \left( \frac{\Delta \Gamma_j}{\Gamma_{\max}} \right) \left( \frac{\eta_j - \eta_i}{r_{ij}^2} \right) \quad (A1)$$

where the maximum value of circulation  $\Gamma_{\max}$  can be written in terms of the lift coefficient and angle of attack as

$$\Gamma_{\max} = \left( \frac{2V_0}{\pi} \right) (c_{av}) (c_{L\alpha}) \alpha \quad (A2)$$

Substituting equation (A2) in (A1) for  $\Gamma_{\max}$  and solving for  $d\epsilon_w/d\alpha$  which is assumed to be  $\frac{d(w_w/V_0)}{d\alpha}$

$$\frac{d\epsilon_w}{d\alpha} = \left( \frac{2c_{L\alpha}}{\pi^2 b} \right) (c_{av}) \sum_{j=1}^n \left( \frac{\Delta \Gamma_j}{\Gamma_{\max}} \right) \left( \frac{\eta_j - \eta_i}{r_{ij}^2} \right) \quad (A3)$$

where

$$r_{ij}^2 = (\eta_j - \eta_i)^2 + \gamma_i^2$$

and

$b$  wing span

$\Delta \Gamma_j$  incremental change in circulation assumed positive for vortices rotating counterclockwise (the distribution of circulation was assumed to be elliptical)

$\eta_i$	lateral distance in semispans from body axis to station <i>i</i>
$\eta_j$	lateral distance in semispans from body axis to the vortex line <i>j</i>
$\gamma_i$	normal distance in semispans from the extended wing-chord plane to the station <i>i</i>
$V_\infty$	free-stream velocity
$c_{av}$	average chord of the exposed wing panel
$C_{L\alpha}$	theoretical lift-curve slope for the exposed wing panels from references 1 and 2

2. In order to satisfy the boundary conditions that there be no flow through the body surface, it was necessary to place image vortices of each of the wing line vortices within the assumed cylindrical body. These image vortices were located in the extended wing-chord plane at lateral distances  $\eta_j'$  by the expression

$$\eta_j' = \frac{R^2}{\eta_j} \quad (A4)$$

where

$R$  body radius in semispans

$\eta_j'$  lateral distance in semispans from body axis to the image vortex line *j*

The values of  $d\epsilon_i/d\alpha$  contributed by these image vortices were computed as:

$$\frac{d\epsilon_i}{d\alpha} = \left( \frac{2C_{L\alpha}}{\pi^2 b} \right) (c_{av}) \sum_{j=1}^n \left( \frac{\Delta\Gamma_j}{\Gamma_{\max}} \right) \left[ \frac{\eta_j' - \eta_i}{(r_{ij}')^2} \right] \quad (A5)$$

where

$$(r_{ij}')^2 = (\eta_j' - \eta_i)^2 + \gamma_i^2$$

3. In addition to the downwash produced by the wing line vortices and by the images of these vortices, vertical velocities were induced by the body since the body was at an angle of attack. These induced velocities were accounted for by replacing the body by a doublet and by

considering only the component of the free-stream velocity perpendicular to the body axis. The expression for computing  $d\epsilon_b/d\alpha$  induced by the body is given in rectangular coordinates in Appendix A of reference 1 as

$$\frac{d\epsilon_b}{d\alpha} = R^2 \left[ \frac{\gamma_i^2 - \eta_i^2}{(\gamma_i^2 + \eta_i^2)^2} \right] \quad (A6)$$

4. The value of  $d\epsilon/d\alpha$  at each station was computed as the sum of the components given in equations (A3), (A5), and (A6) above as

$$\frac{d\epsilon}{d\alpha} = \frac{d\epsilon_w}{d\alpha} + \frac{d\epsilon_i}{d\alpha} + \frac{d\epsilon_b}{d\alpha} \quad (A7)$$

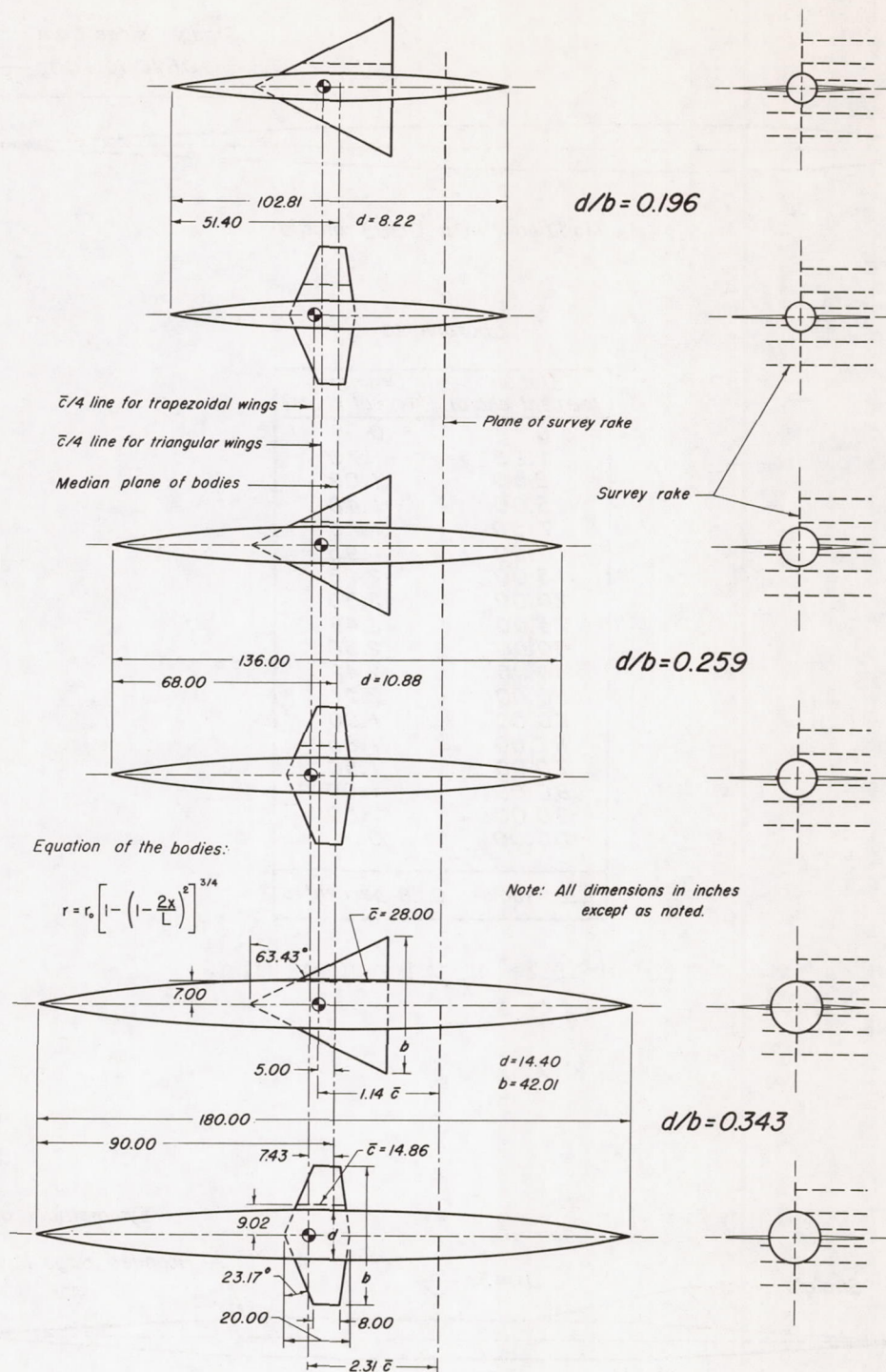
## REFERENCES

1. Hopkins, Edward J., and Carel, Hubert C.: Experimental and Theoretical Study of the Effect of Body Size on the Aerodynamic Characteristics of an Aspect Ratio 3.0 Wing-Body Combination. NACA RM A51G24, 1951.
2. Hopkins, Edward J., and Carel, Hubert C.: Experimental and Theoretical Study of the Interference at Low Speed Between Slender Bodies and Triangular Wings. NACA RM A53A14, 1953.
3. Rogers, Arthur Wm.: Application of Two-Dimensional Vortex Theory to the Prediction of Flow Fields Behind Wings of Wing-Body Combinations at Subsonic and Supersonic Speeds. NACA TN 3227, 1954.
4. Swanson, Robert S., and Gillis, Clarence L.: Wind-Tunnel Calibration and Corrections Procedures for Three-Dimensional Models. NACA WR L-1, 1944 (Supersedes NACA ARR L4E31.)
5. Swanson, Robert S., and Schuldenfrei, Marvin S.: Jet Boundary Corrections to the Downwash Behind Powered Models in Rectangular Wind Tunnels with Numerical Values for 7- by 10-Foot Closed Wind Tunnels. NACA WR L-711, 1942.
6. Spreiter, John R., and Sacks, Alvin H.: The Rolling Up of the Trailing Vortex Sheet and Its Effect on the Downwash Behind Wings. Jour. Aero. Sci., vol. 18, no. 1, Jan. 1951, Preprint 250.
7. Spreiter, John R.: Aerodynamic Properties of Slender Wing-Body Combinations at Subsonic, Transonic, and Supersonic Speeds. NACA TN 1662, 1948.

TABLE I.- DOWNWASH FIGURE INDEX

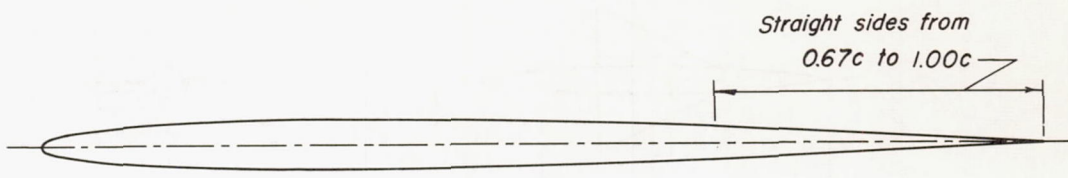
Fig. no.	$i_w$ , deg	$\frac{d}{b}$	Aspect ratio	Fig. no.	$i_w$ , deg	$\frac{d}{b}$	Aspect ratio
5(a)	0	0.196	2.0	8(a)	0	0.196	3.0
5(b)	2			8(b)	2		
5(c)	4			8(c)	4		
5(d)	6			8(d)	6		
5(e)	8			8(e)	8		
5(f)	10			8(f)	10		
6(a)	0	.259	2.0	9(a)	0	.259	3.0
6(b)	2			9(b)	2		
6(c)	4			9(c)	4		
6(d)	6			9(d)	6		
6(e)	8			9(e)	8		
6(f)	10			9(f)	10		
7(a)	0	.343	2.0	10(a)	0	.343	3.0
7(b)	2			10(b)	2		
7(c)	4			10(c)	4		
7(d)	6			10(d)	6		
7(e)	8			10(e)	8		
7(f)	10			10(f)	10		





(a) Rake locations and model plan forms.

Figure 1.- Dimensional data for the wing-body combinations.



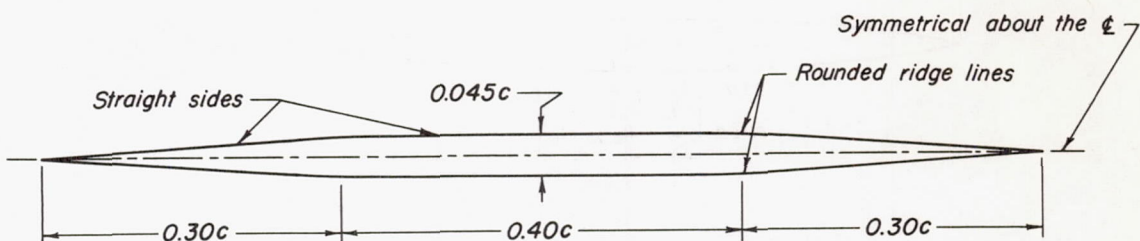
Modified NACA 0005 profile

## Coordinates

Station (percent chord)	Ordinate (percent chord)
0	0
1.25	.79
2.50	1.09
5.00	1.48
7.50	1.75
10.00	1.95
15.00	2.23
20.00	2.39
25.00	2.48
30.00	2.50
40.00	2.42
50.00	2.21
60.00	1.90
67.00	1.65
70.00	1.50
80.00	1.00
90.00	.50
100.00	0

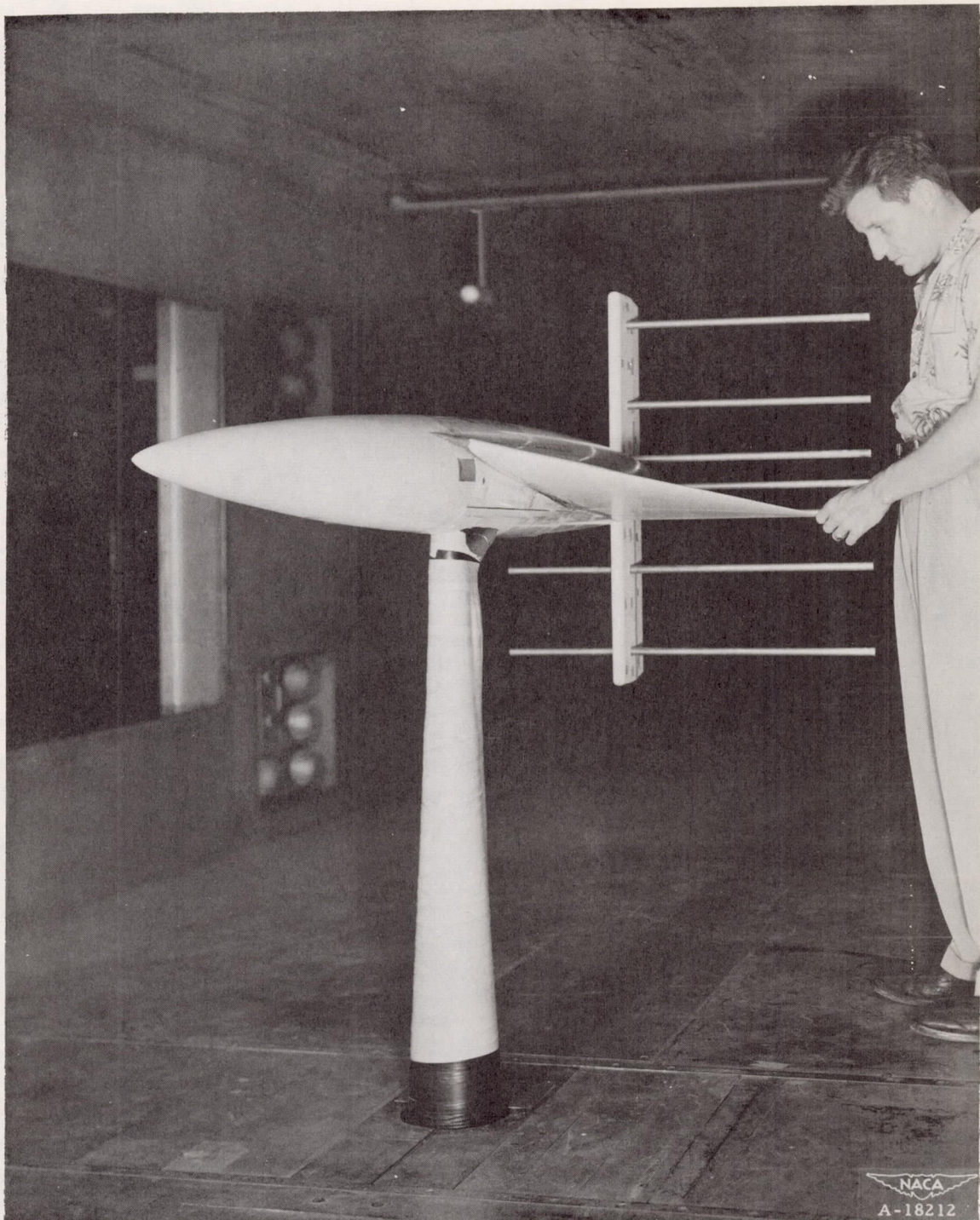
L.E. radius: 0.28 percent c

(b) Profile of triangular wing.



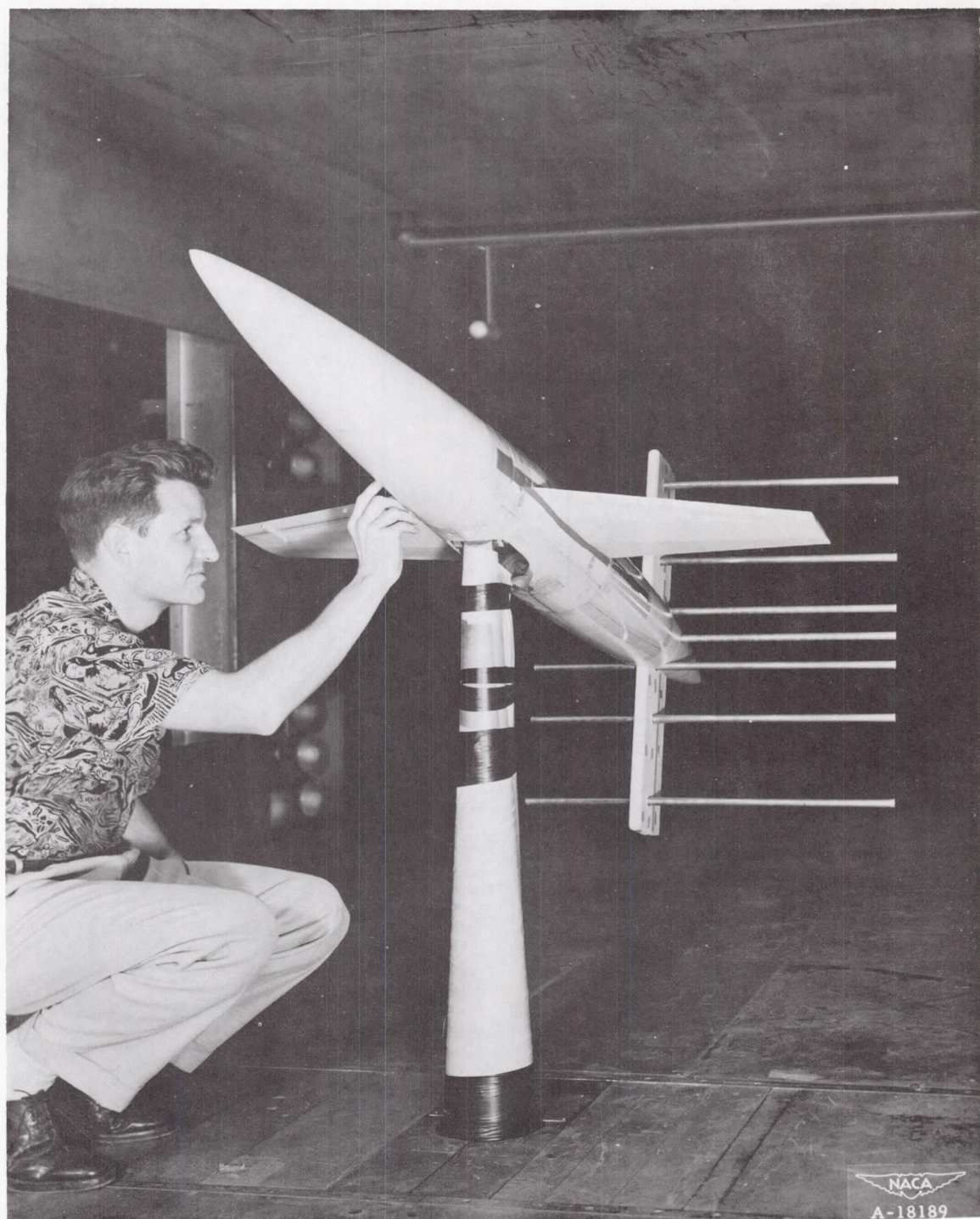
(c) Profile of trapezoidal wing.

Figure 1.- Concluded.



(a) Triangular wing.

Figure 2.- Wing-body combinations with survey rake in one of the Ames 7- by 10-foot wind tunnels.



(b) Trapezoidal wing.

Figure 2.- Concluded.

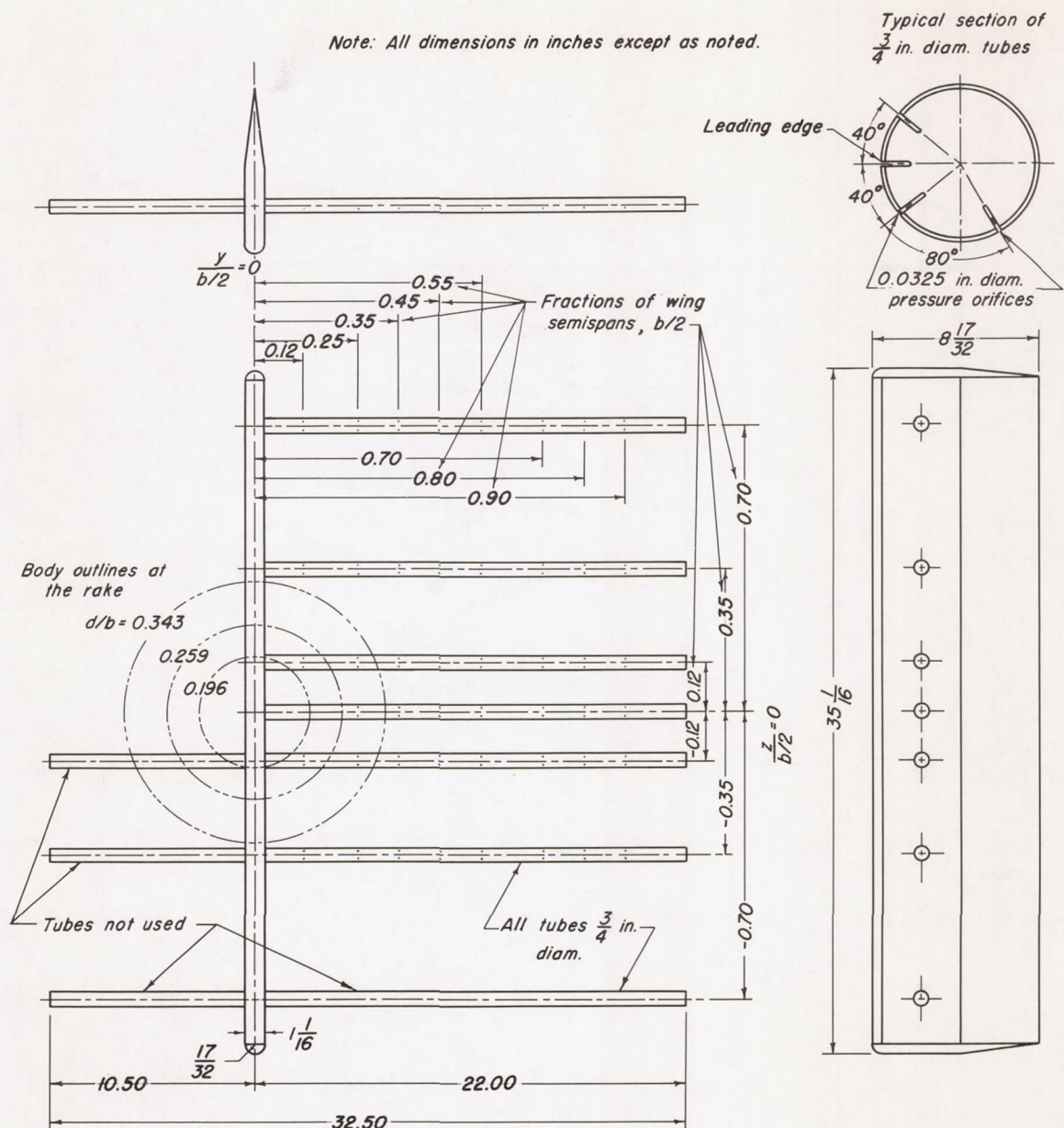


Figure 3.- Dimensional sketch of survey rake.

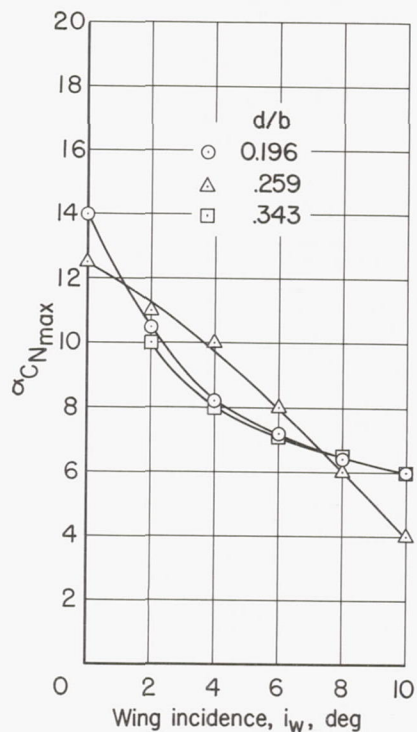


Figure 4.- Effect of wing-incidence change on  $\alpha_{C_N\max}$  for the wing-body combination having the trapezoidal wing.

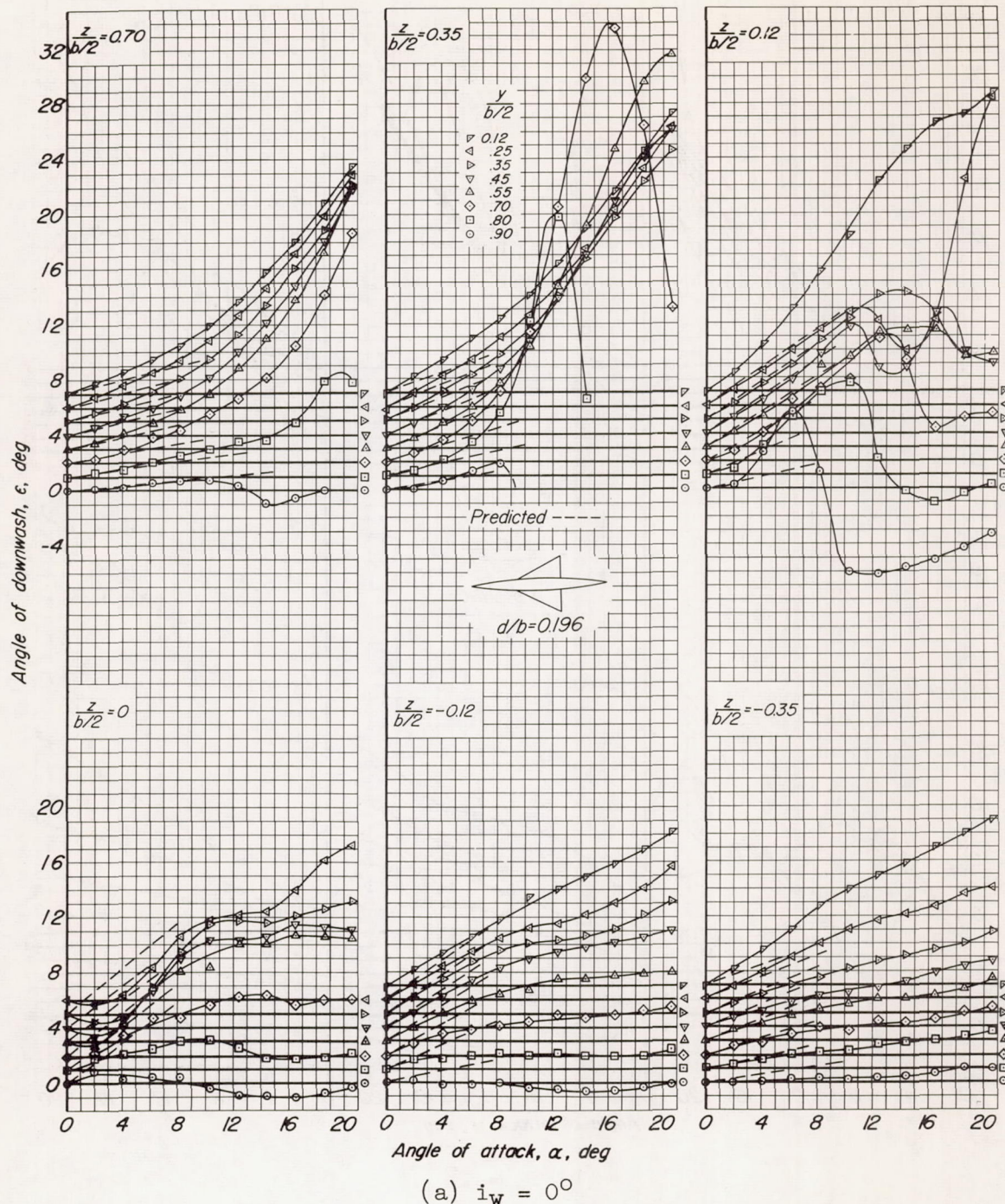


Figure 5.- Downwash in a plane  $1.14\bar{c}$  behind the  $0.25\bar{c}$  line of the triangular wing of the wing-body combination having a ratio of maximum body diameter to wing span of 0.196.

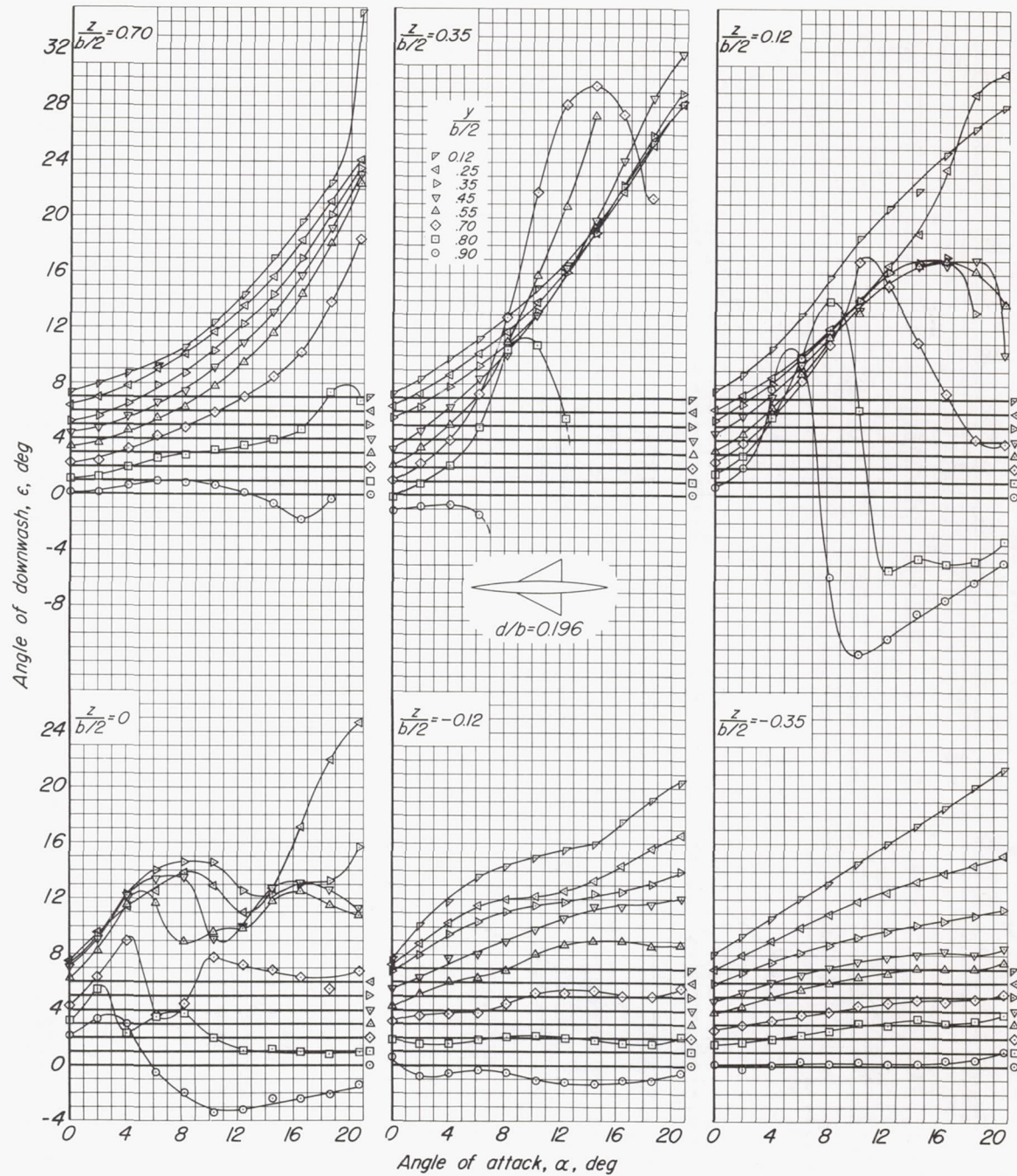


Figure 5.- Continued.

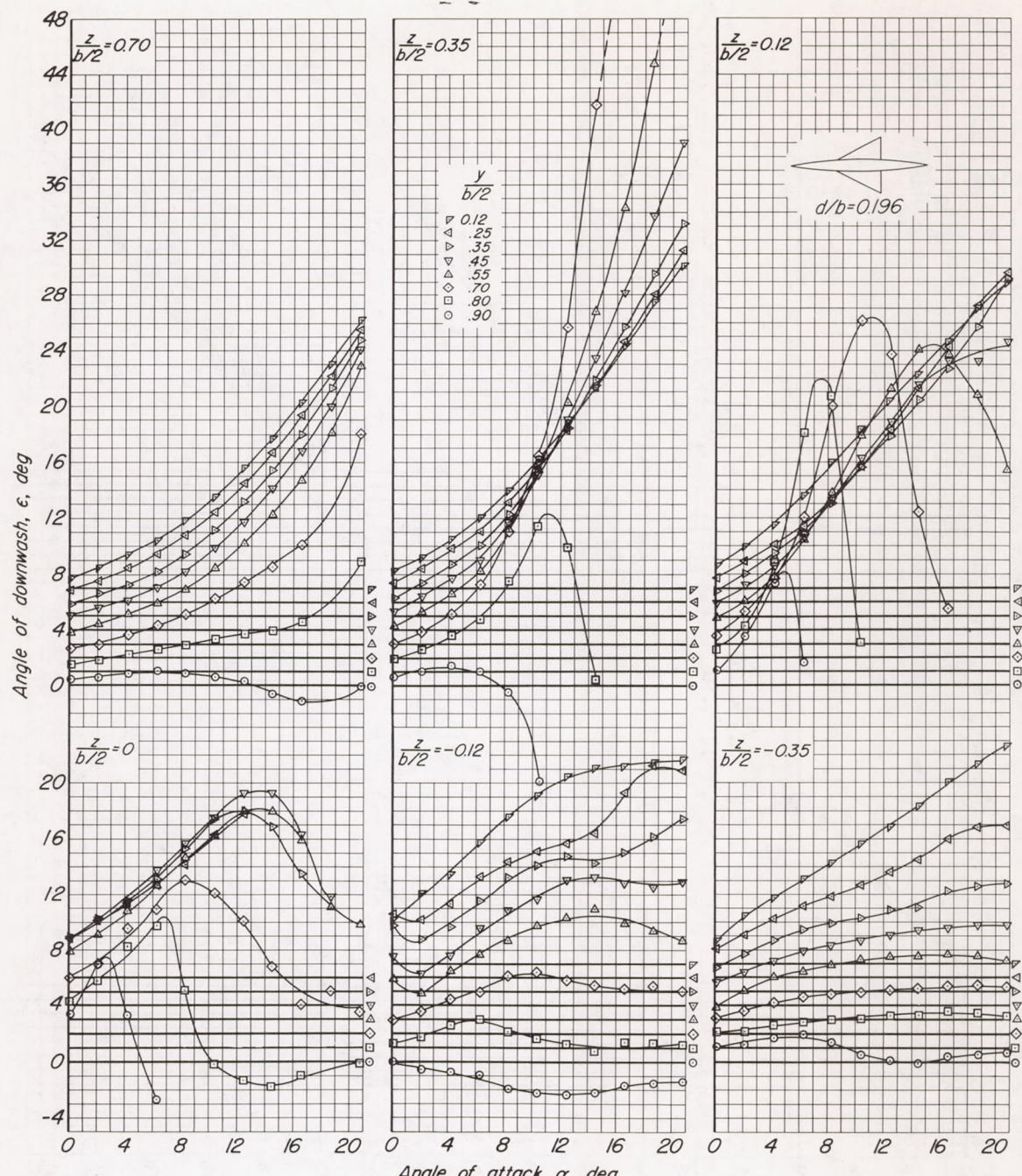
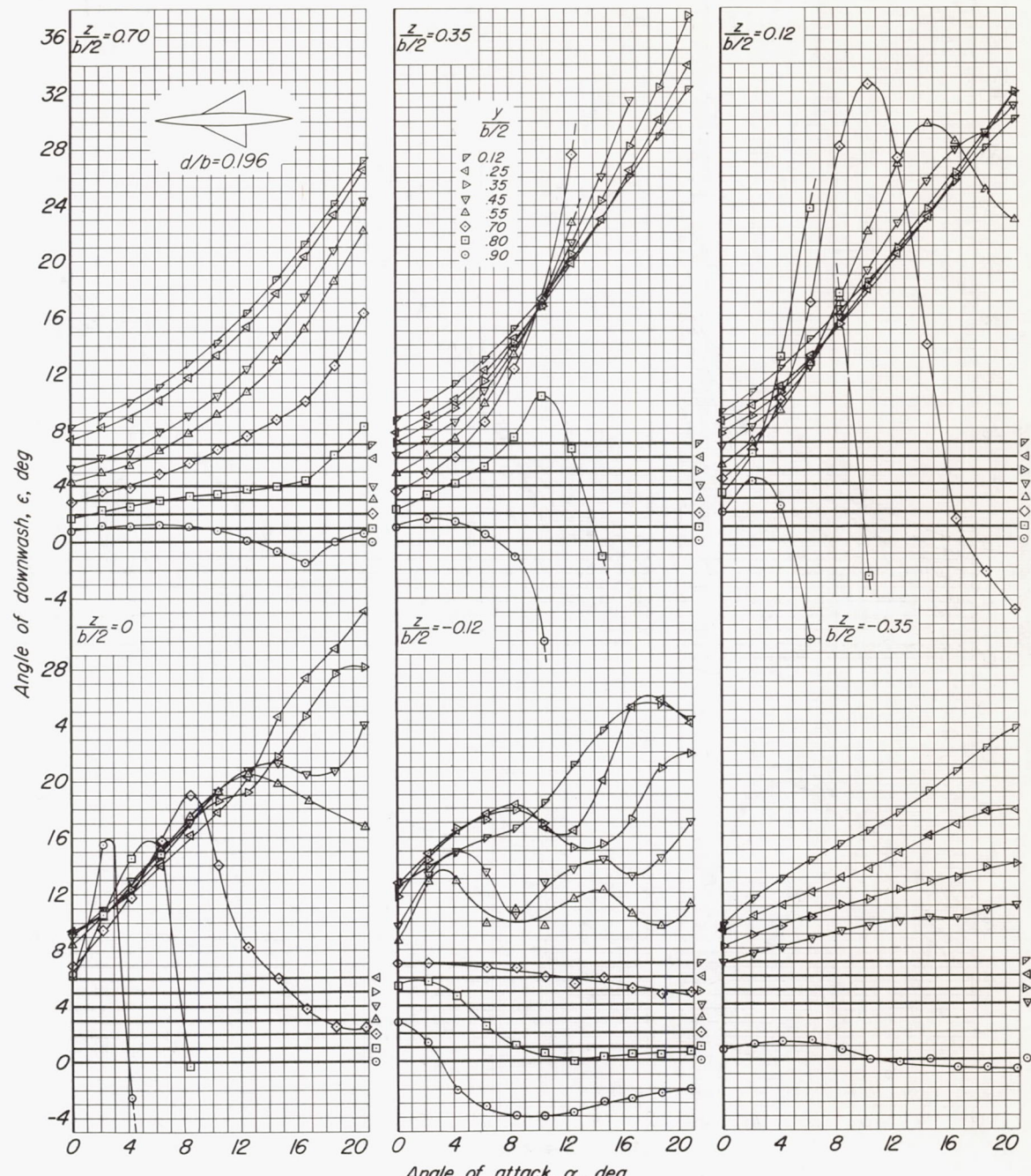
(c)  $i_W = 4^\circ$ 

Figure 5.- Continued.



(d)  $i_W = 6^\circ$

Figure 5.- Continued.

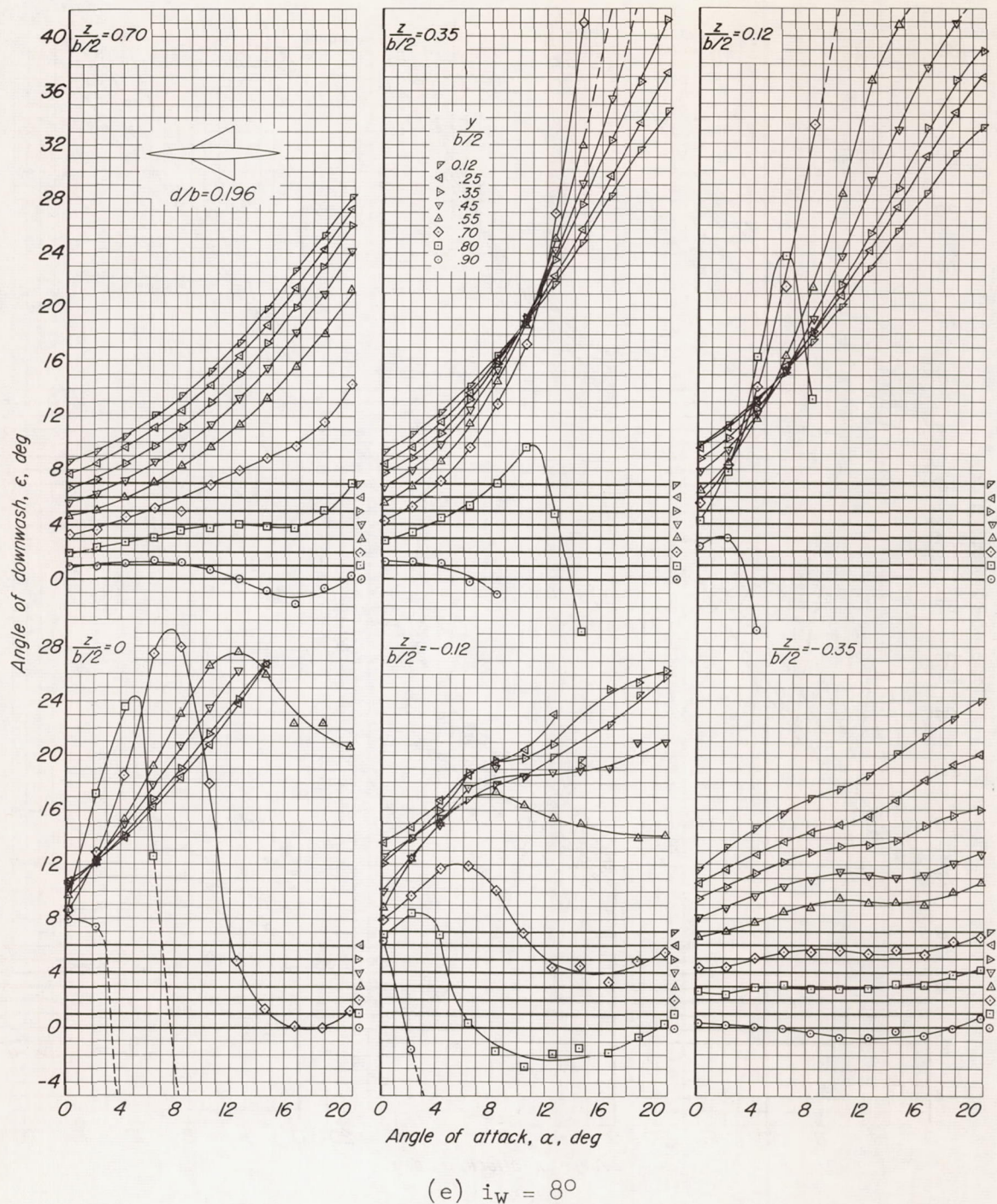


Figure 5.- Continued.

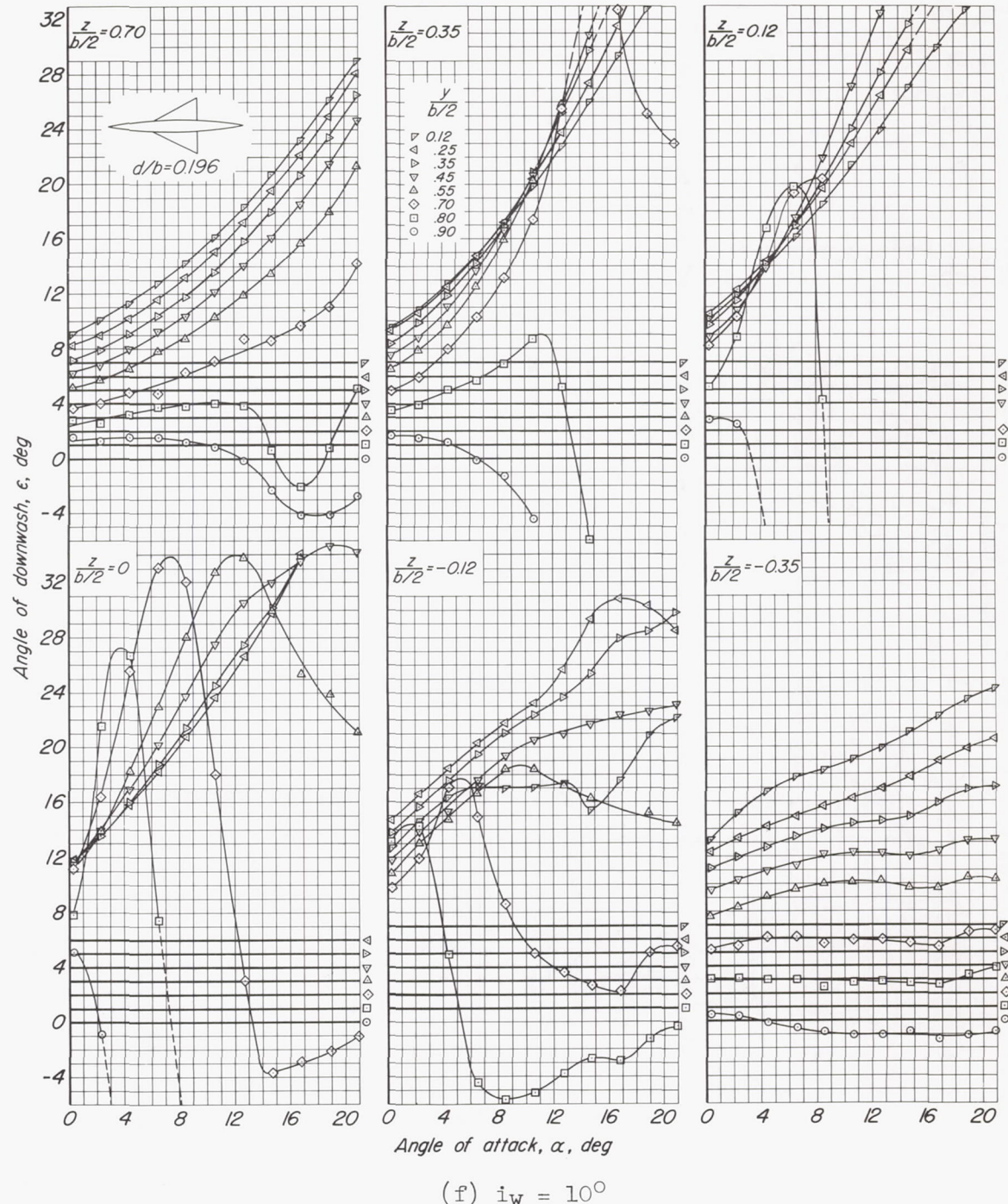


Figure 5.- Concluded.

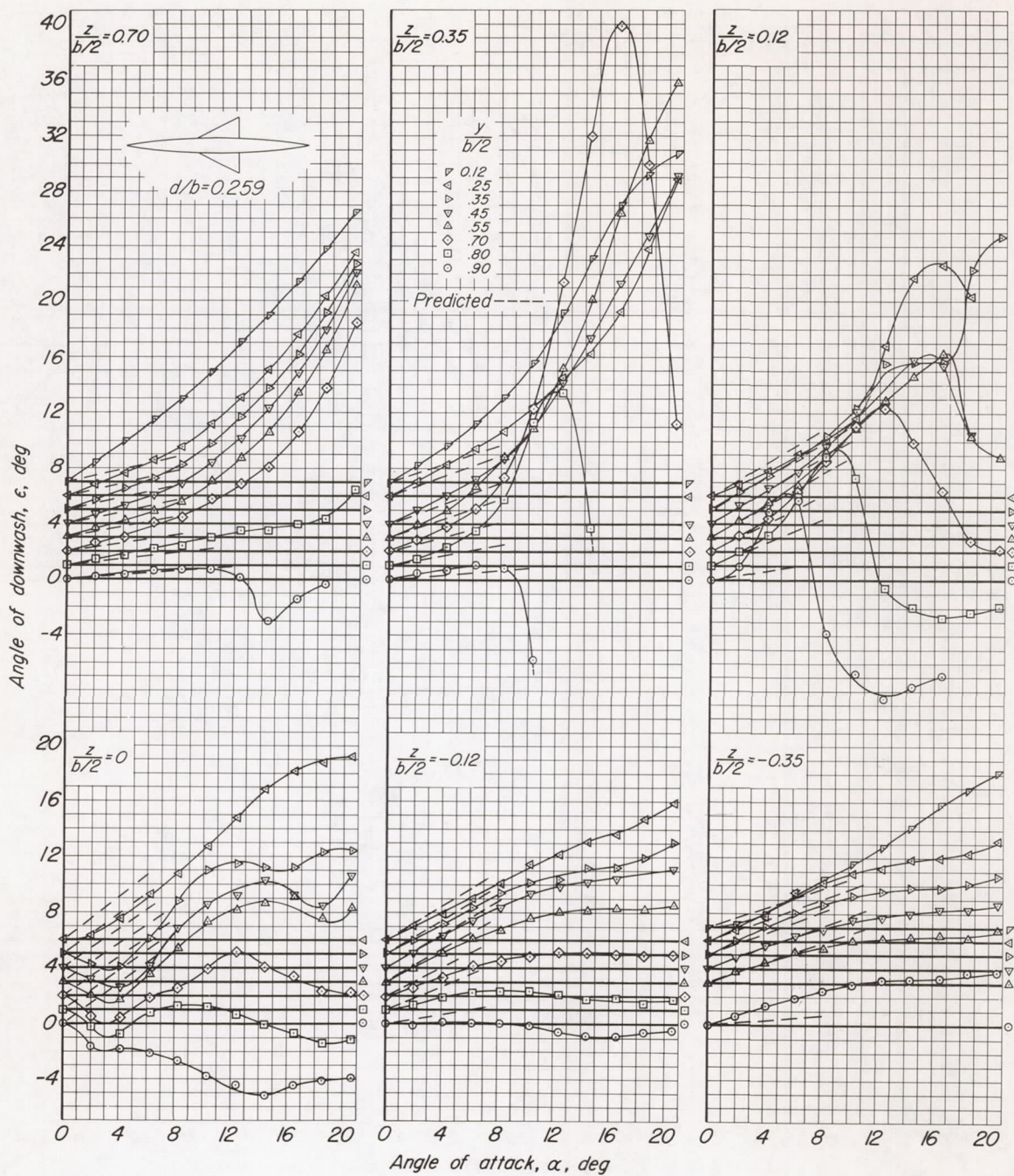
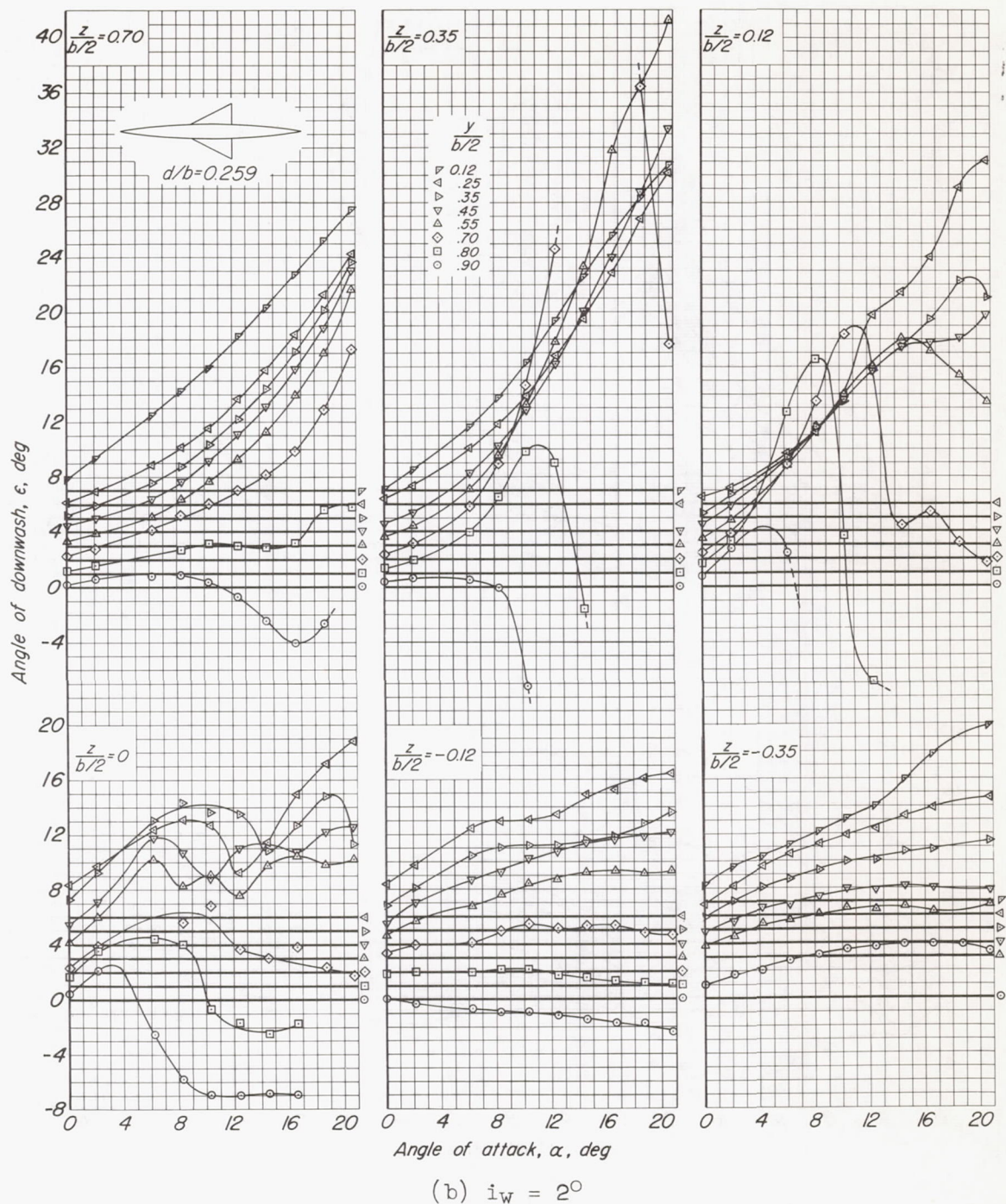
(a)  $i_w = 0^\circ$ 

Figure 6.- Downwash in a plane  $1.14\bar{c}$  behind the  $0.25\bar{c}$  line of the triangular wing of the wing-body combination having a ratio of maximum body diameter to wing span of 0.259.



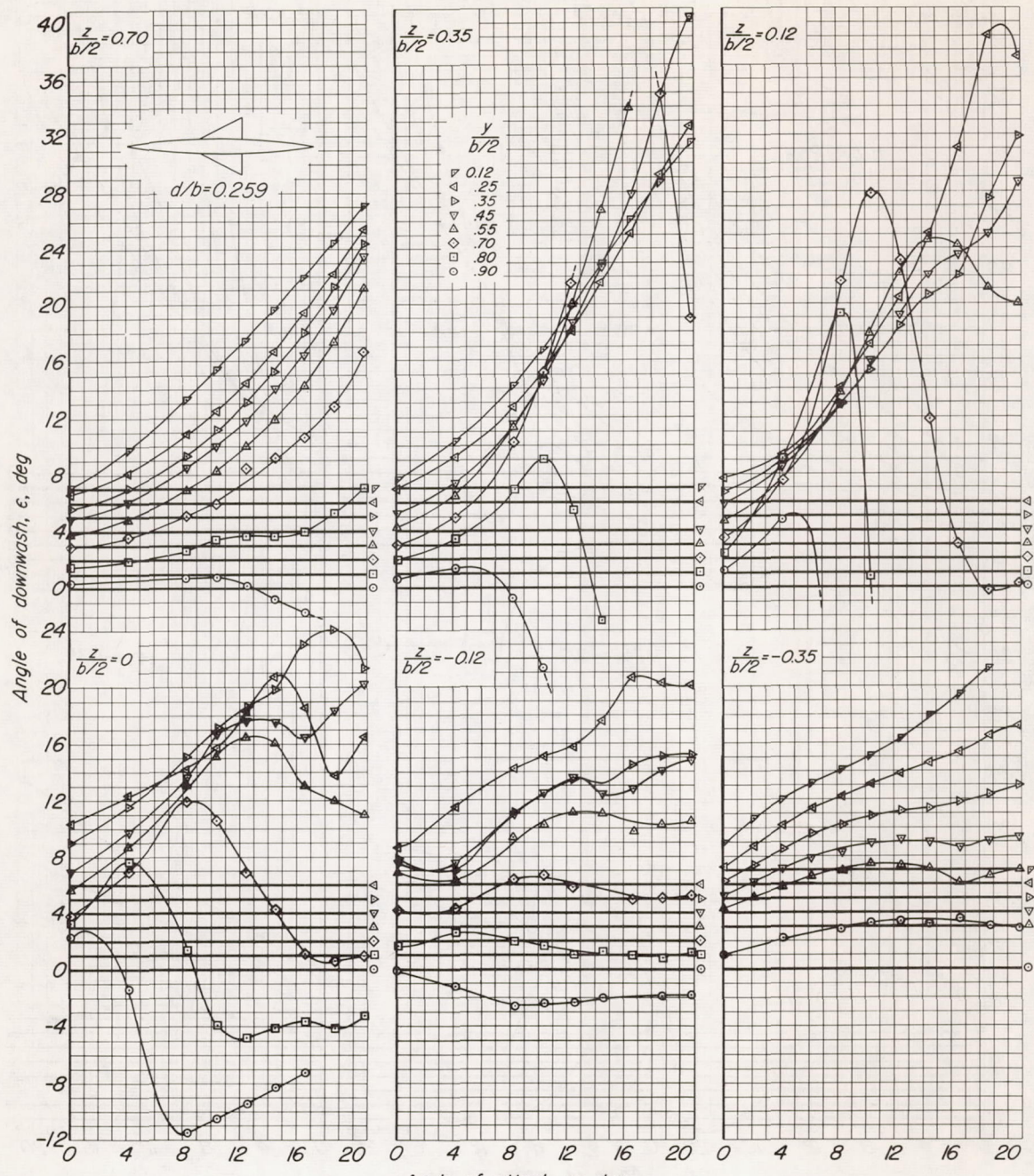
(c)  $i_w = 40^\circ$ 

Figure 6.- Continued.

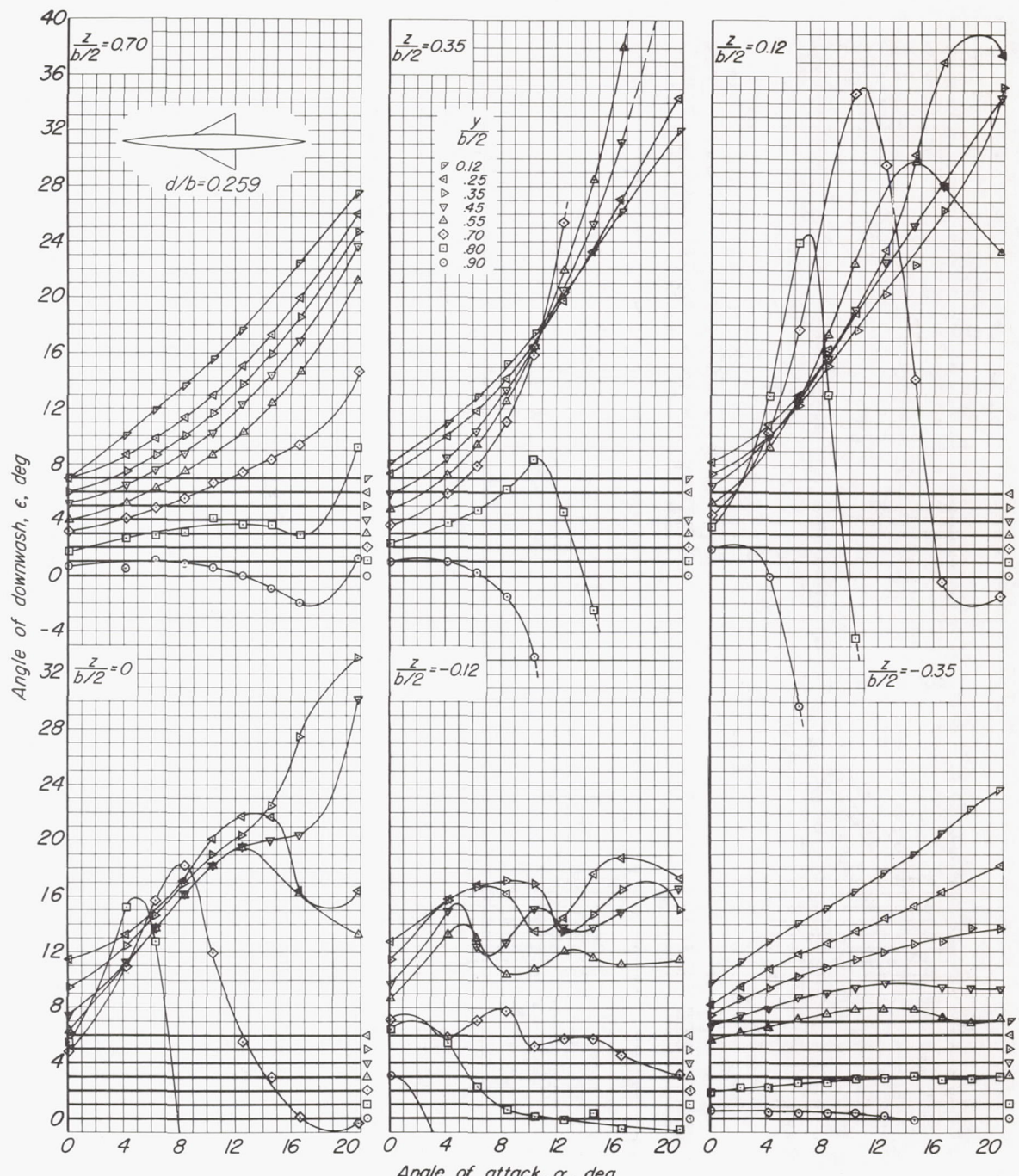
(d)  $i_w = 6^\circ$ 

Figure 6.- Continued.

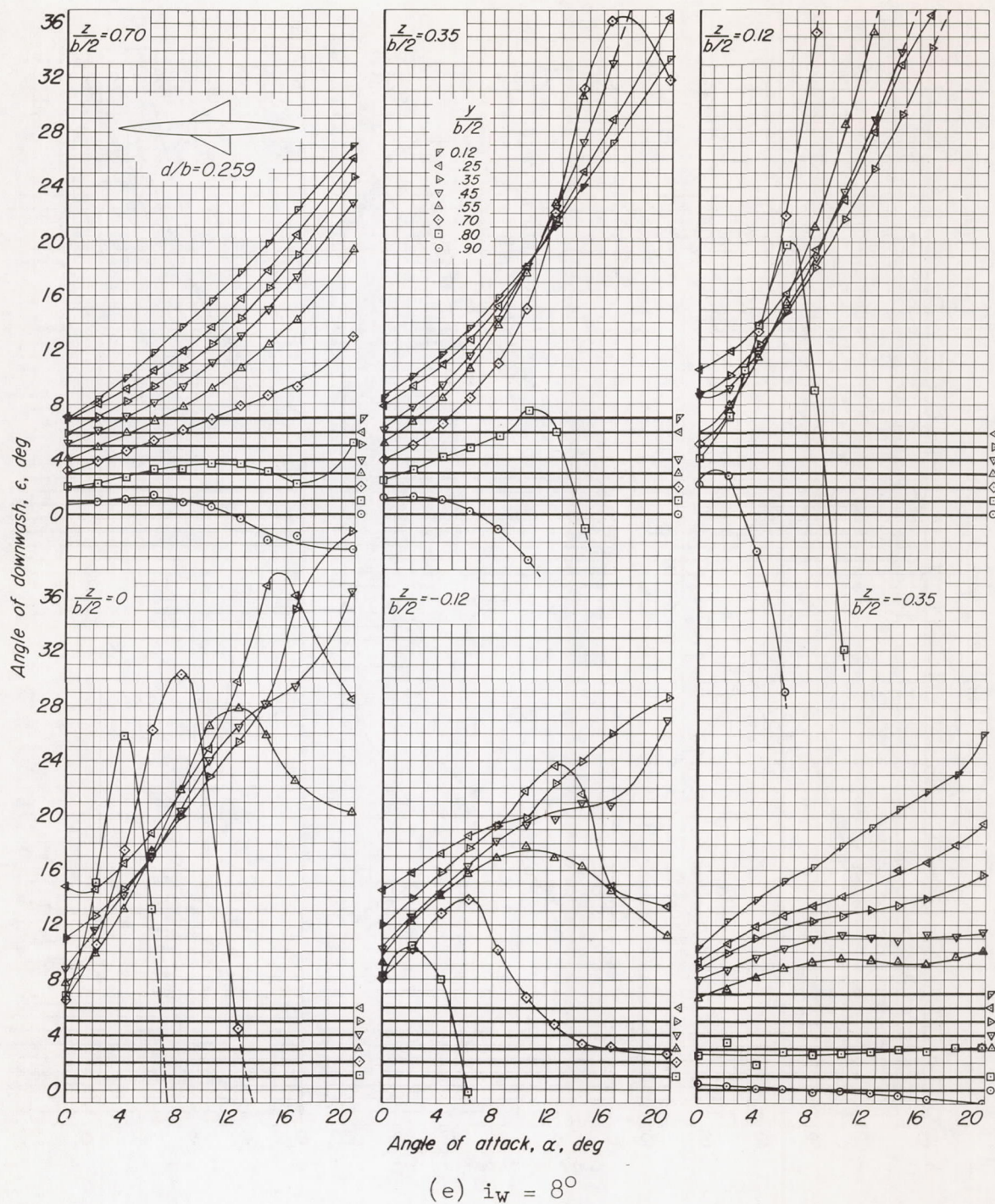


Figure 6.- Continued.

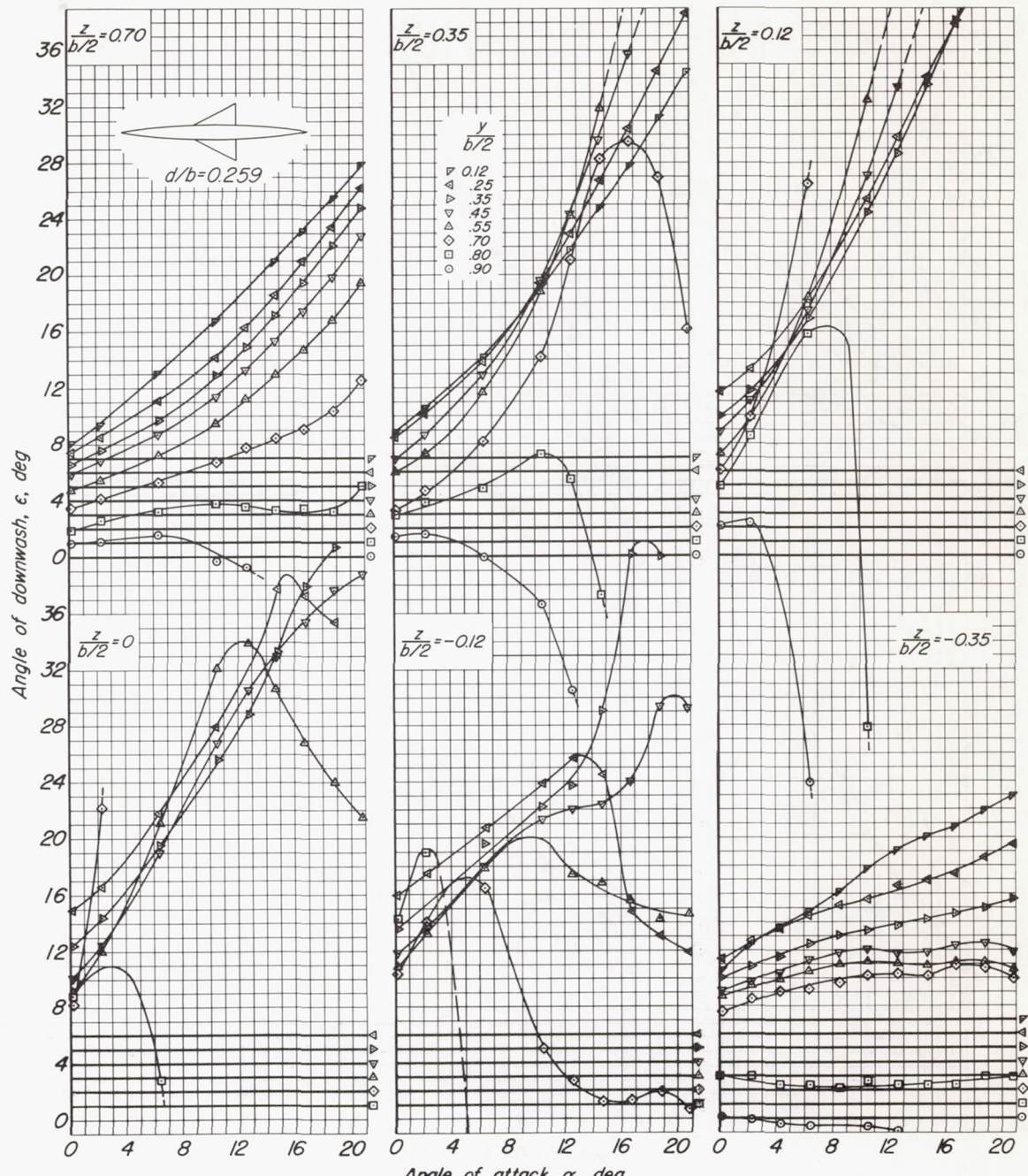
(f)  $i_w = 10^\circ$ 

Figure 6.- Concluded.

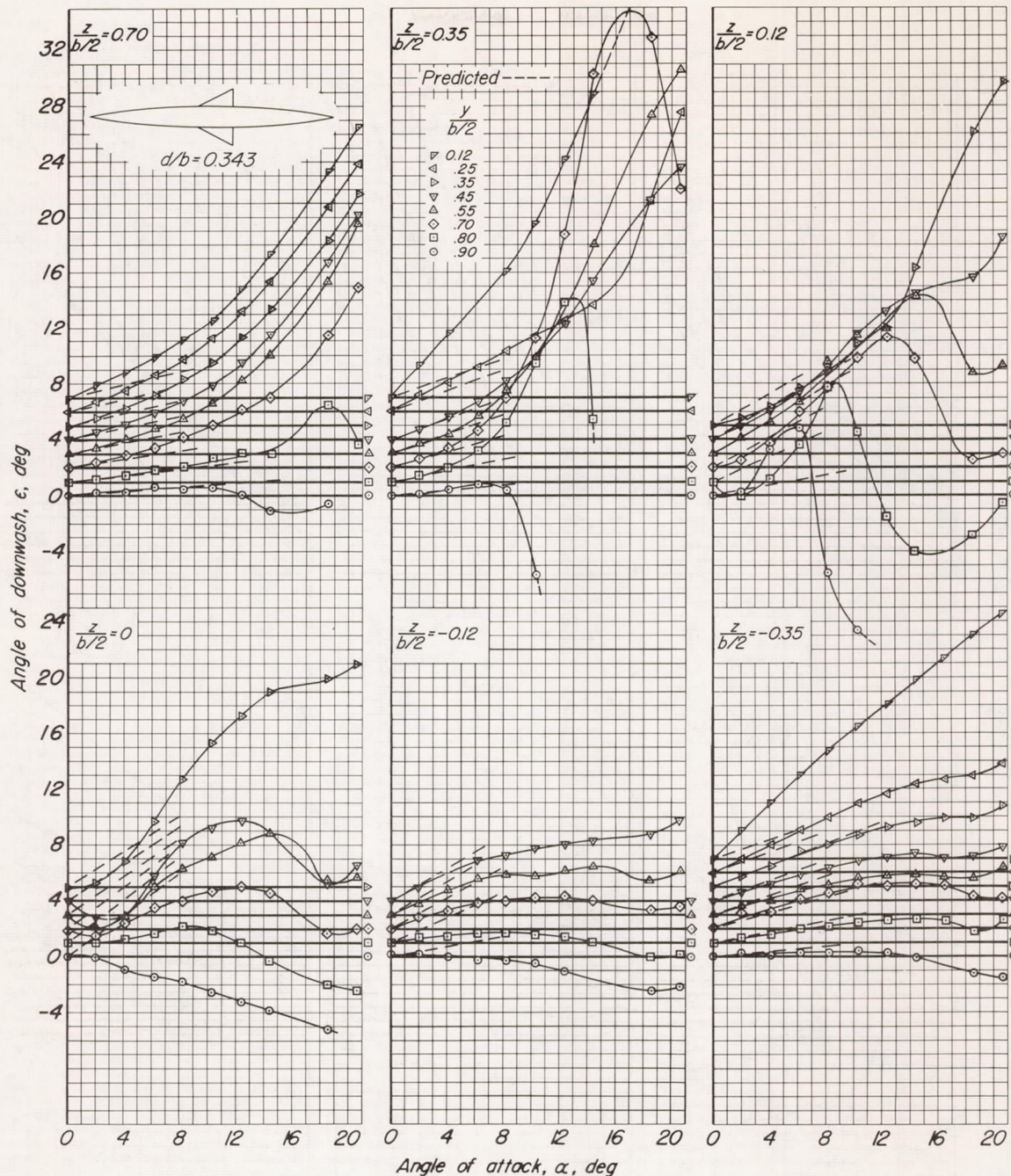
(a)  $i_w = 0^\circ$ 

Figure 7.- Downwash in a plane  $1.14\bar{c}$  behind the  $0.25\bar{c}$  line of the triangular wing of the wing-body combination having a ratio of maximum body diameter to wing span of  $0.343$ .

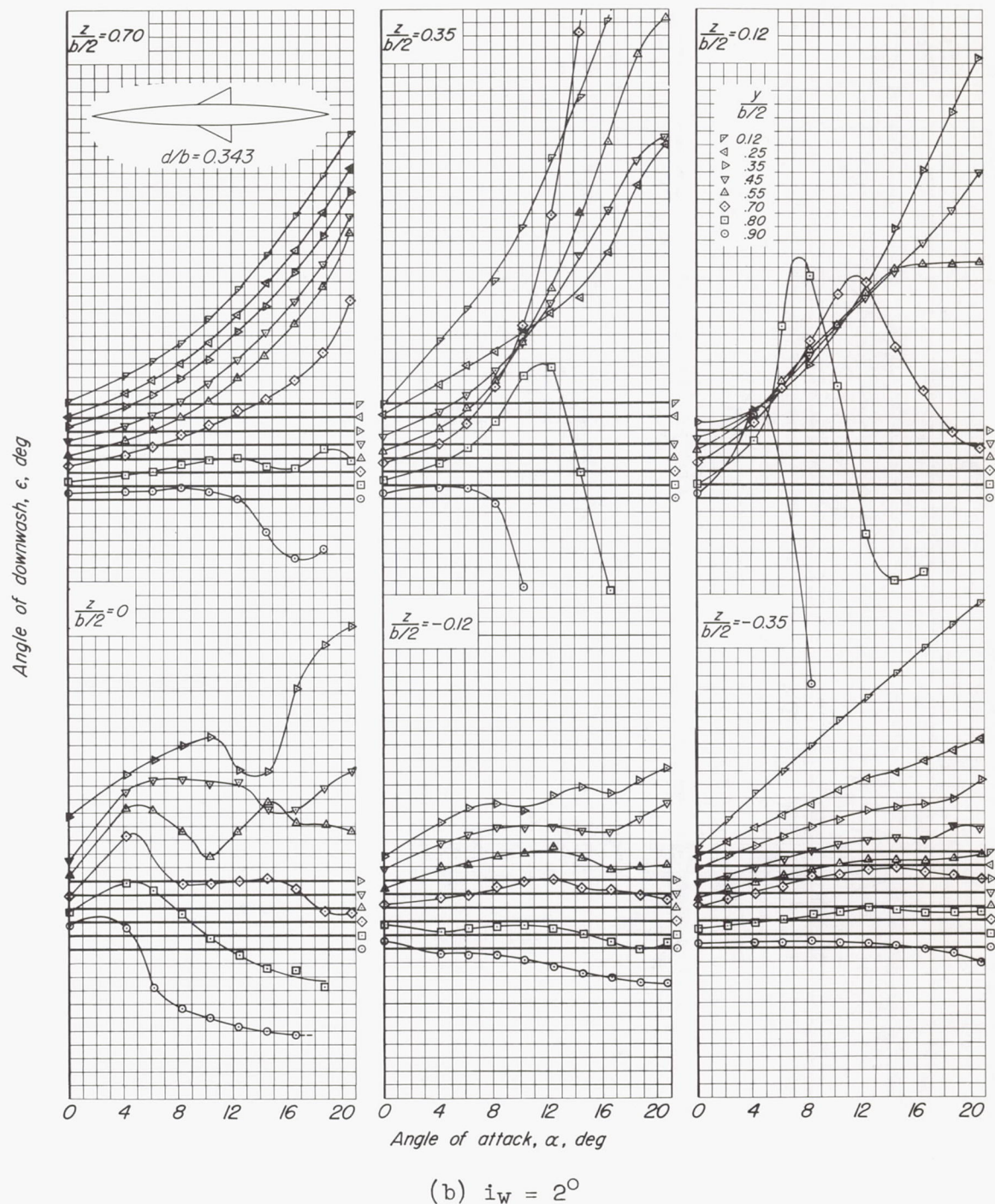


Figure 7.- Continued.

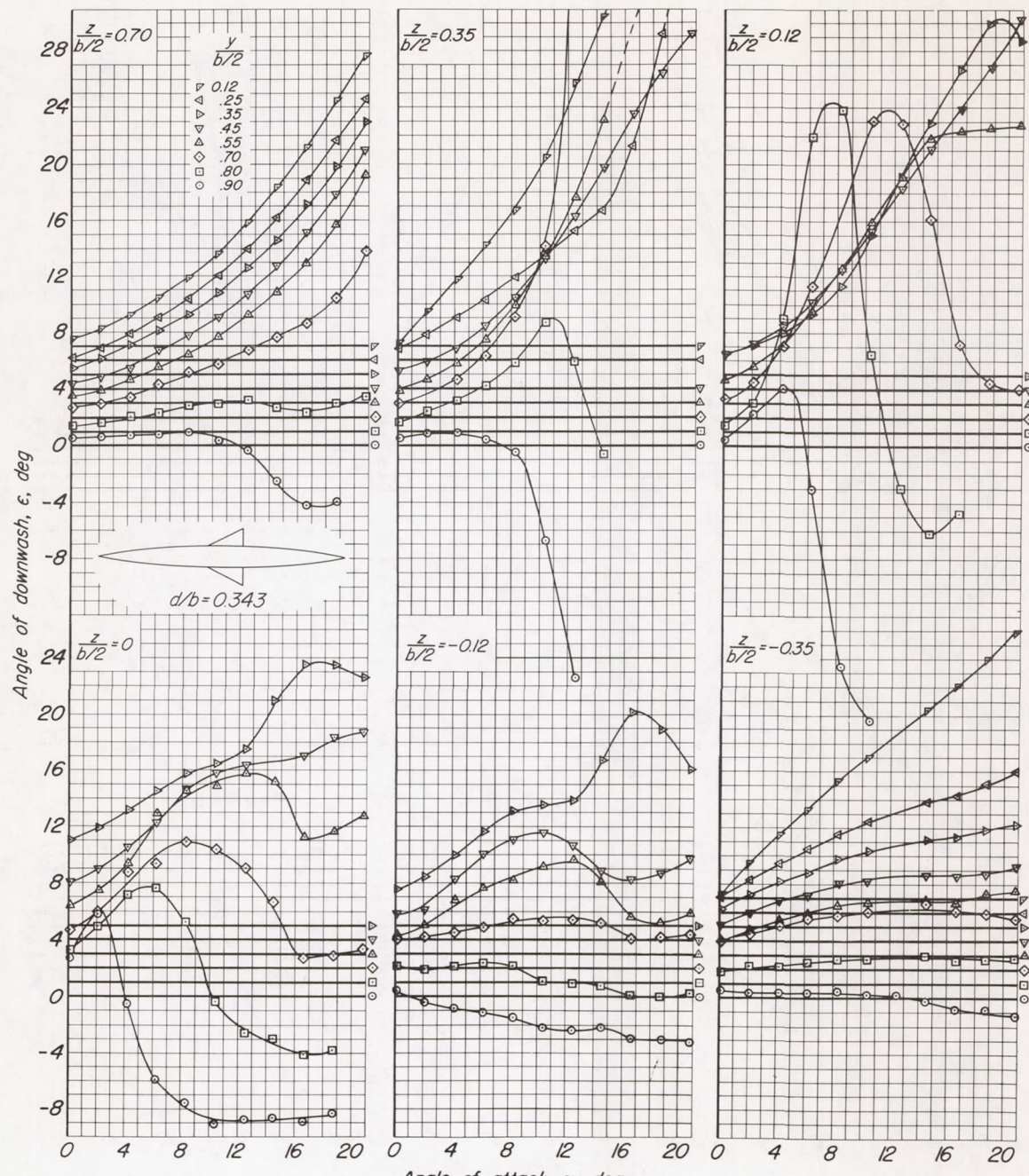
(c)  $i_w = 4^\circ$ 

Figure 7.- Continued.

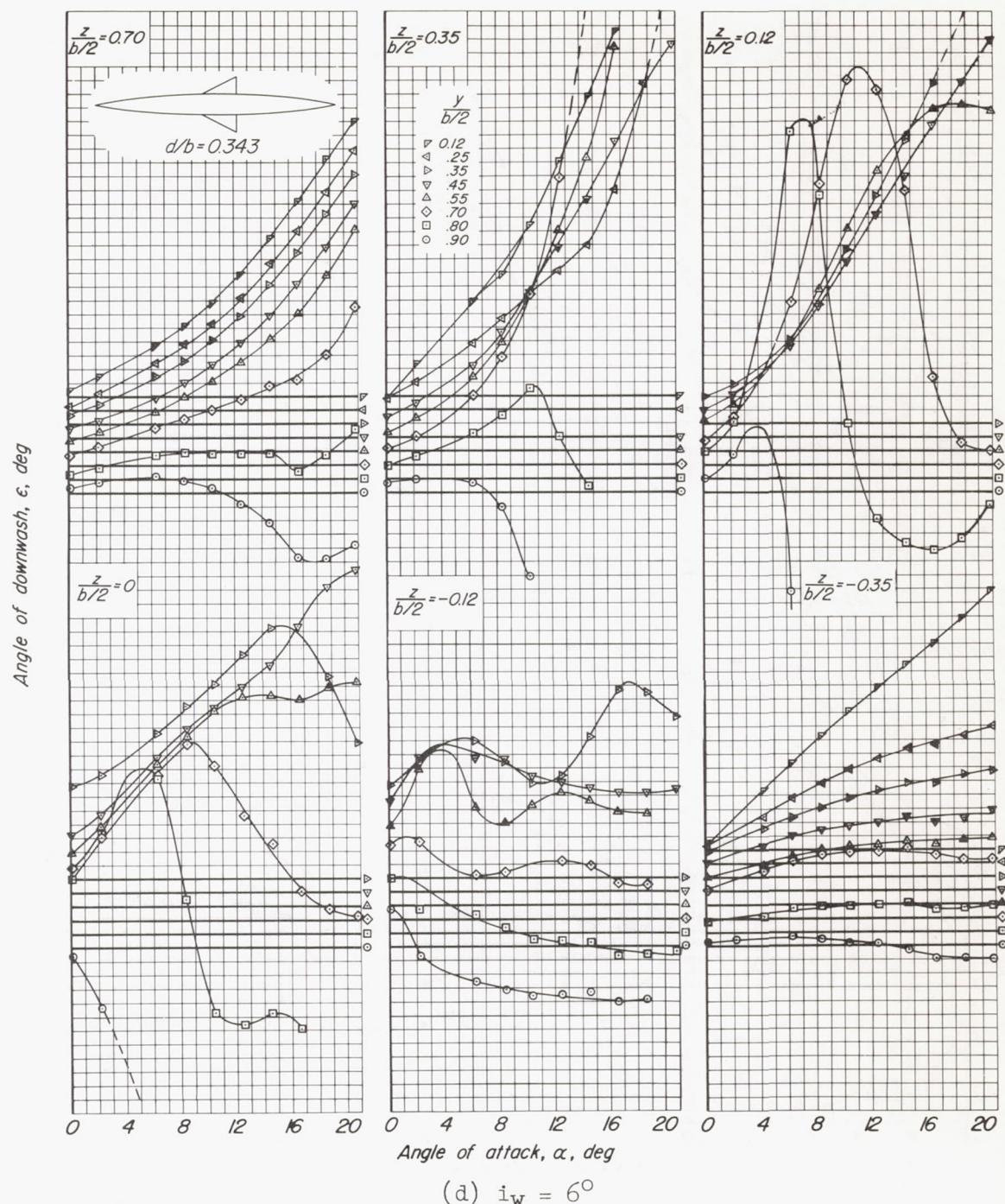


Figure 7.- Continued.

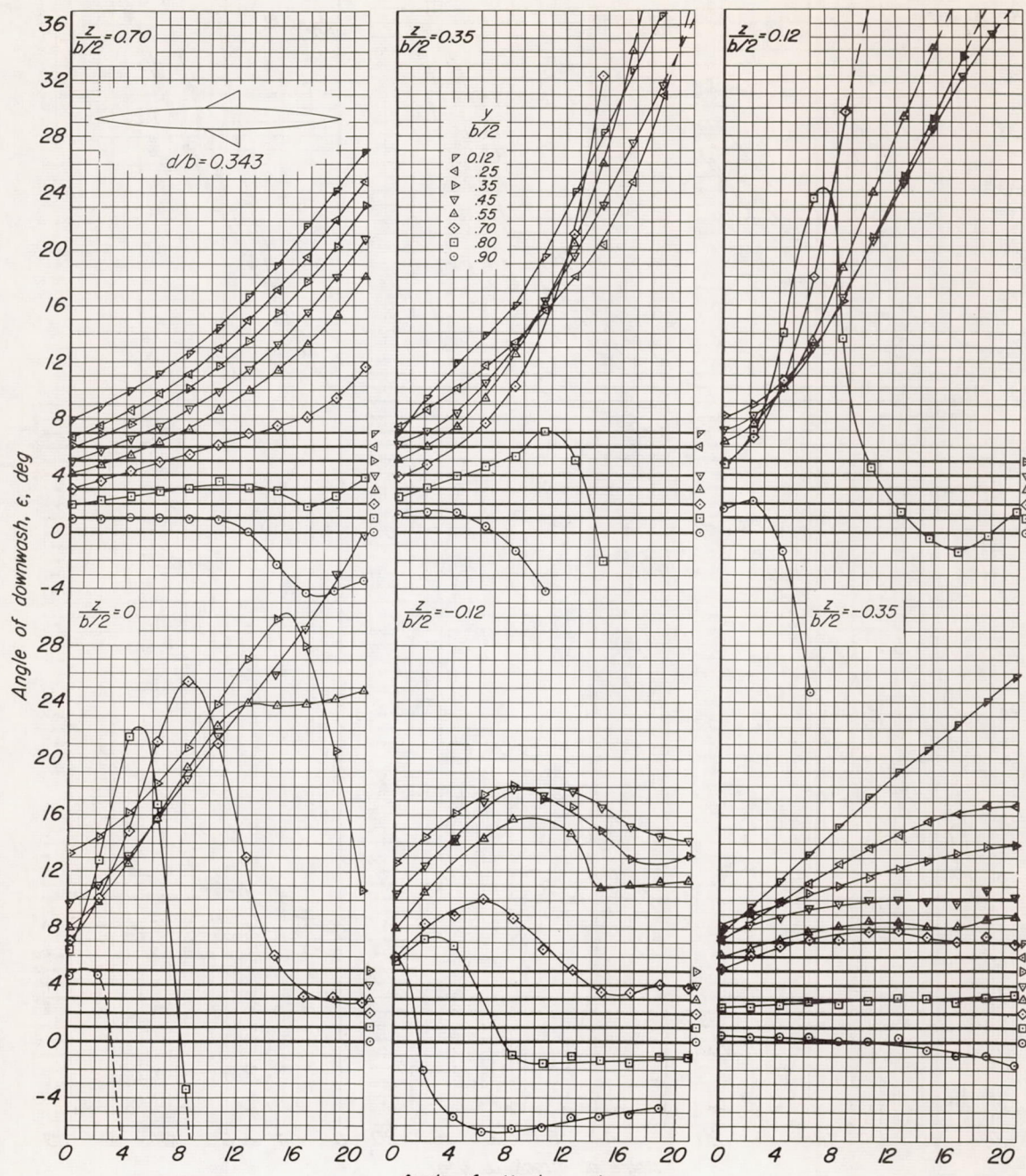
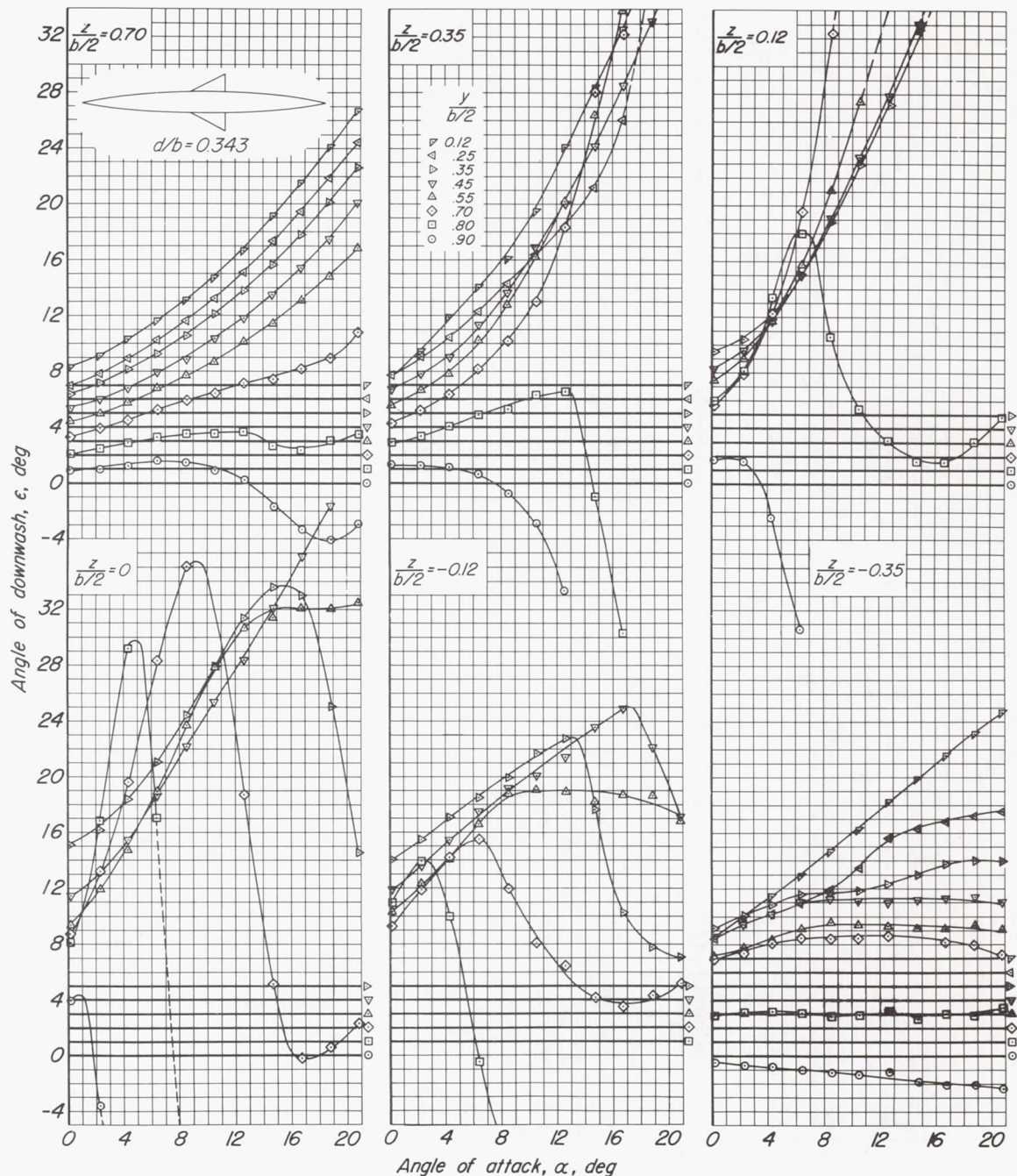
(e)  $i_w = 8^\circ$ 

Figure 7.- Continued.



$$(f) \quad i_w = 10^\circ$$

Figure 7.- Concluded.

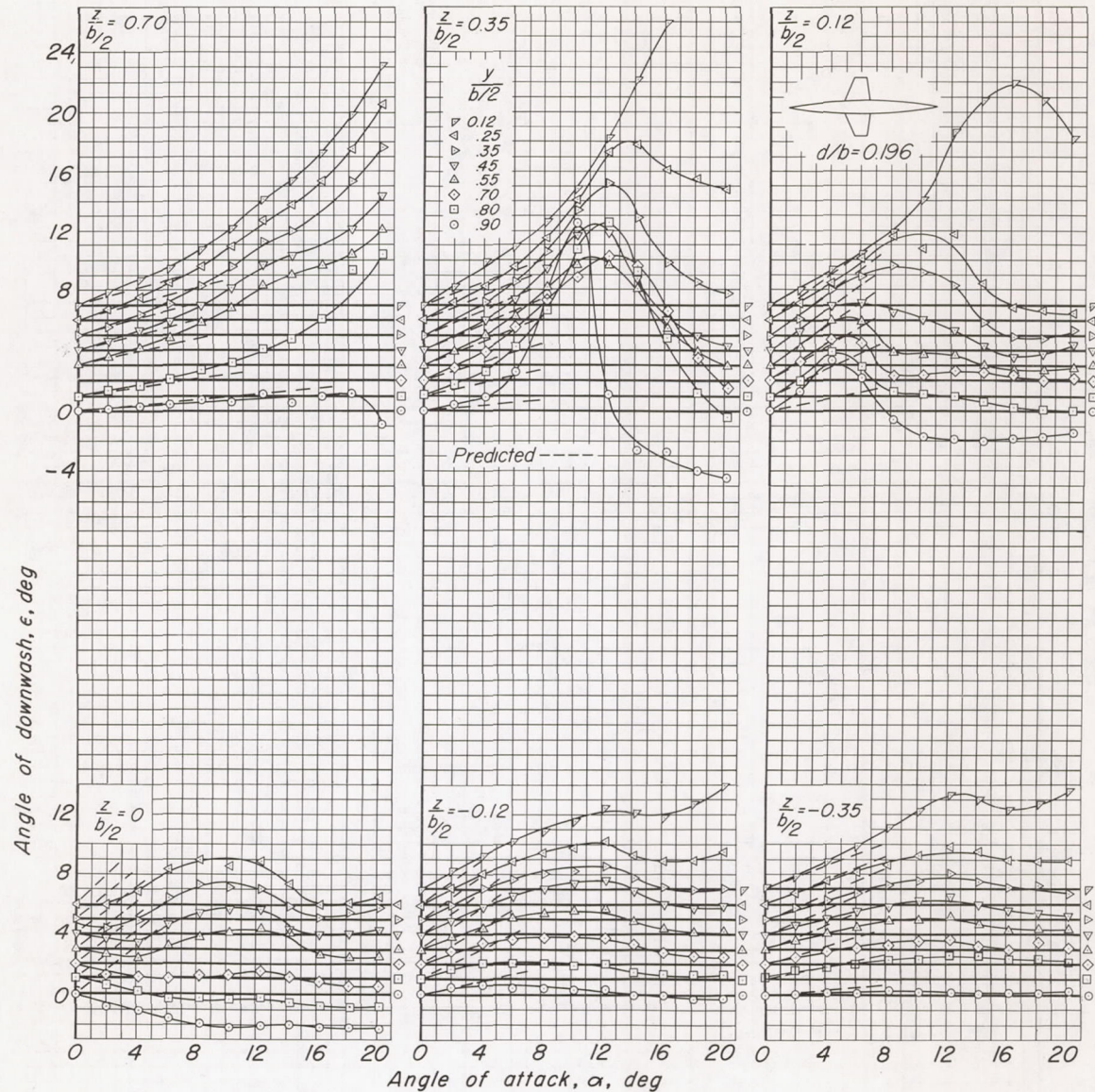
(a)  $i_w = 0^\circ$ 

Figure 8.- Downwash in a plane  $2.31\bar{c}$  behind the  $0.25\bar{c}$  line of the trapezoidal wing of the wing-body combination having a ratio of maximum body diameter to wing span of 0.196.

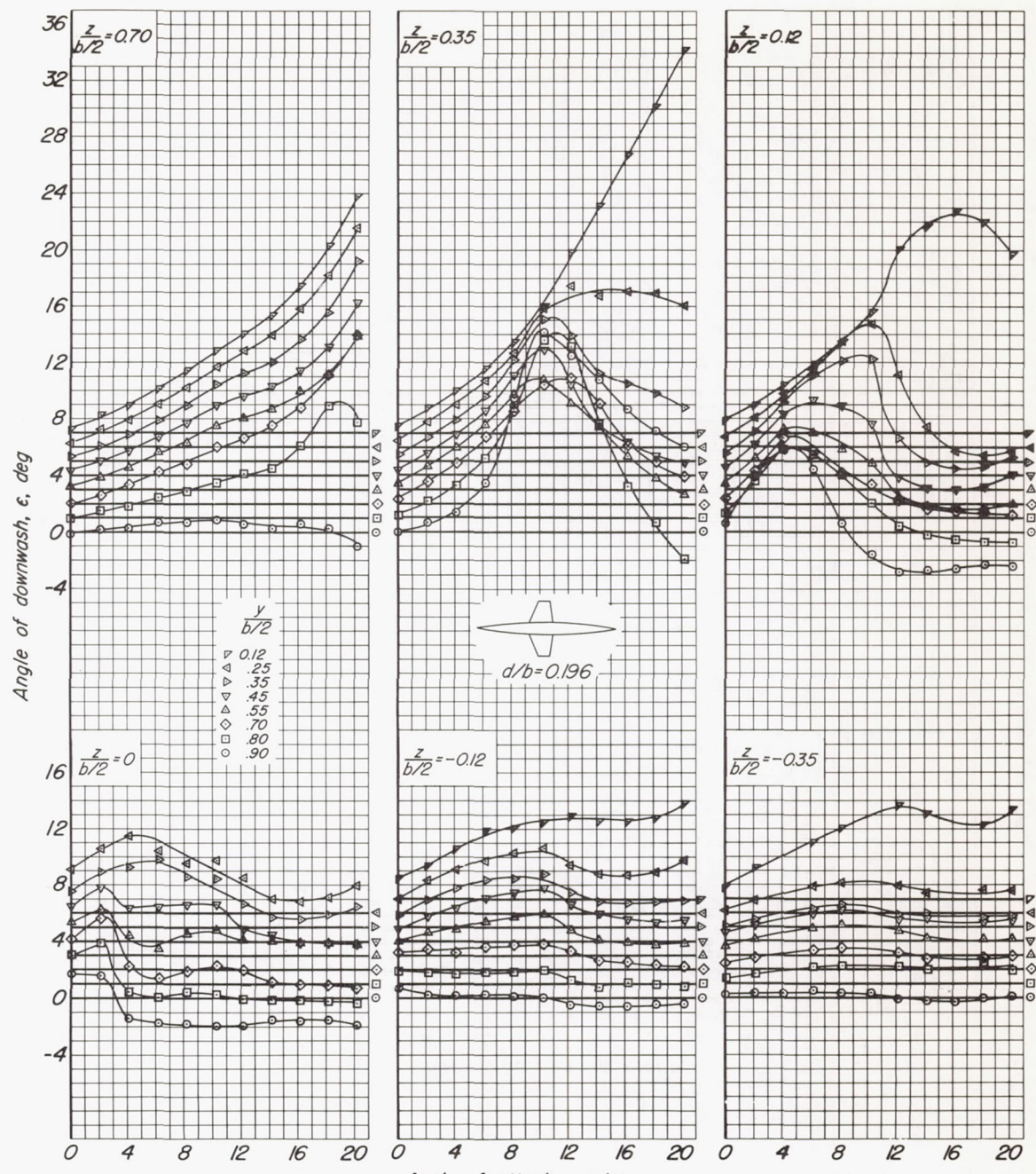
(b)  $i_W = 2^\circ$ 

Figure 8.- Continued.

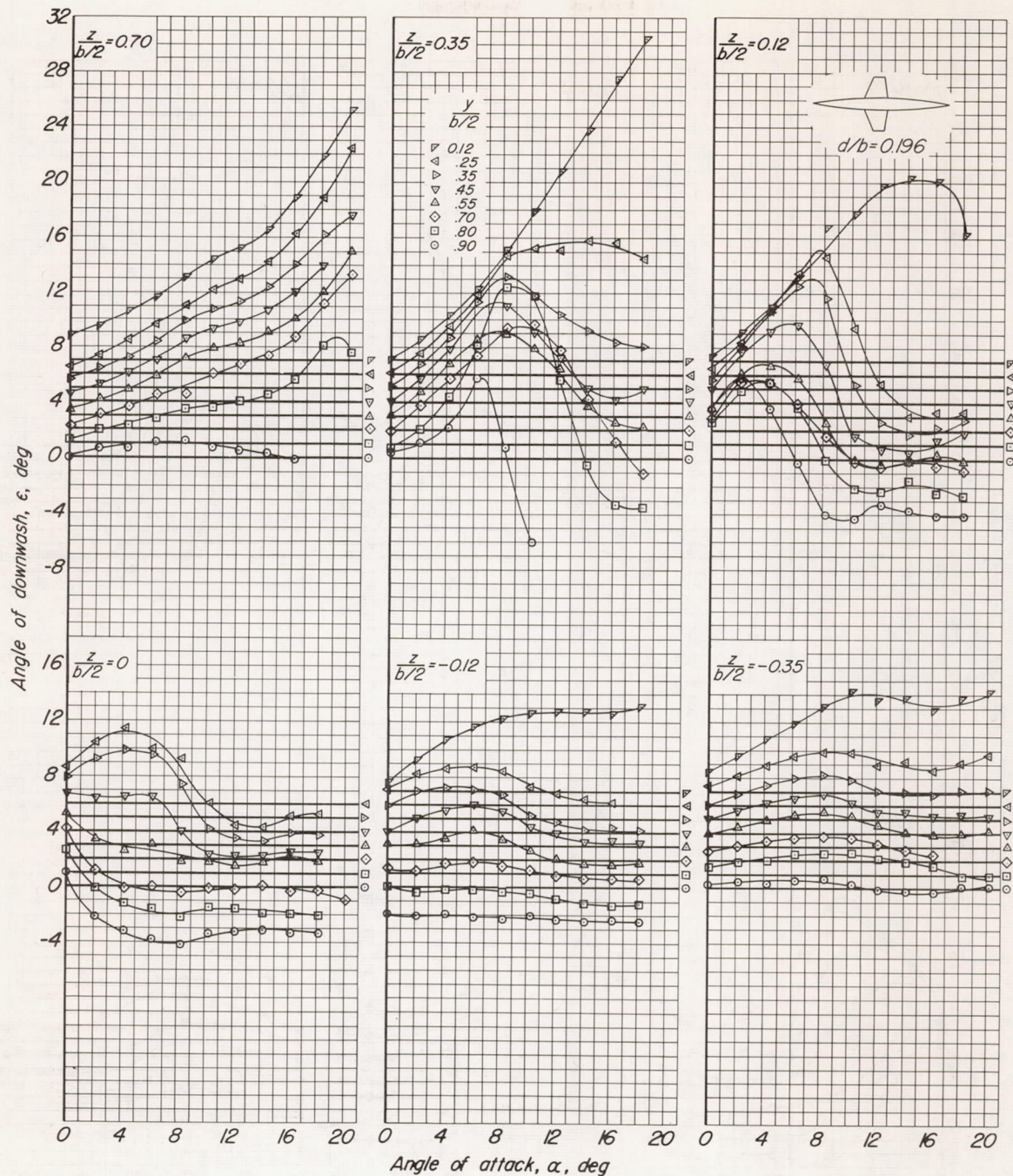
(c)  $i_w = 4^\circ$ 

Figure 8.- Continued.

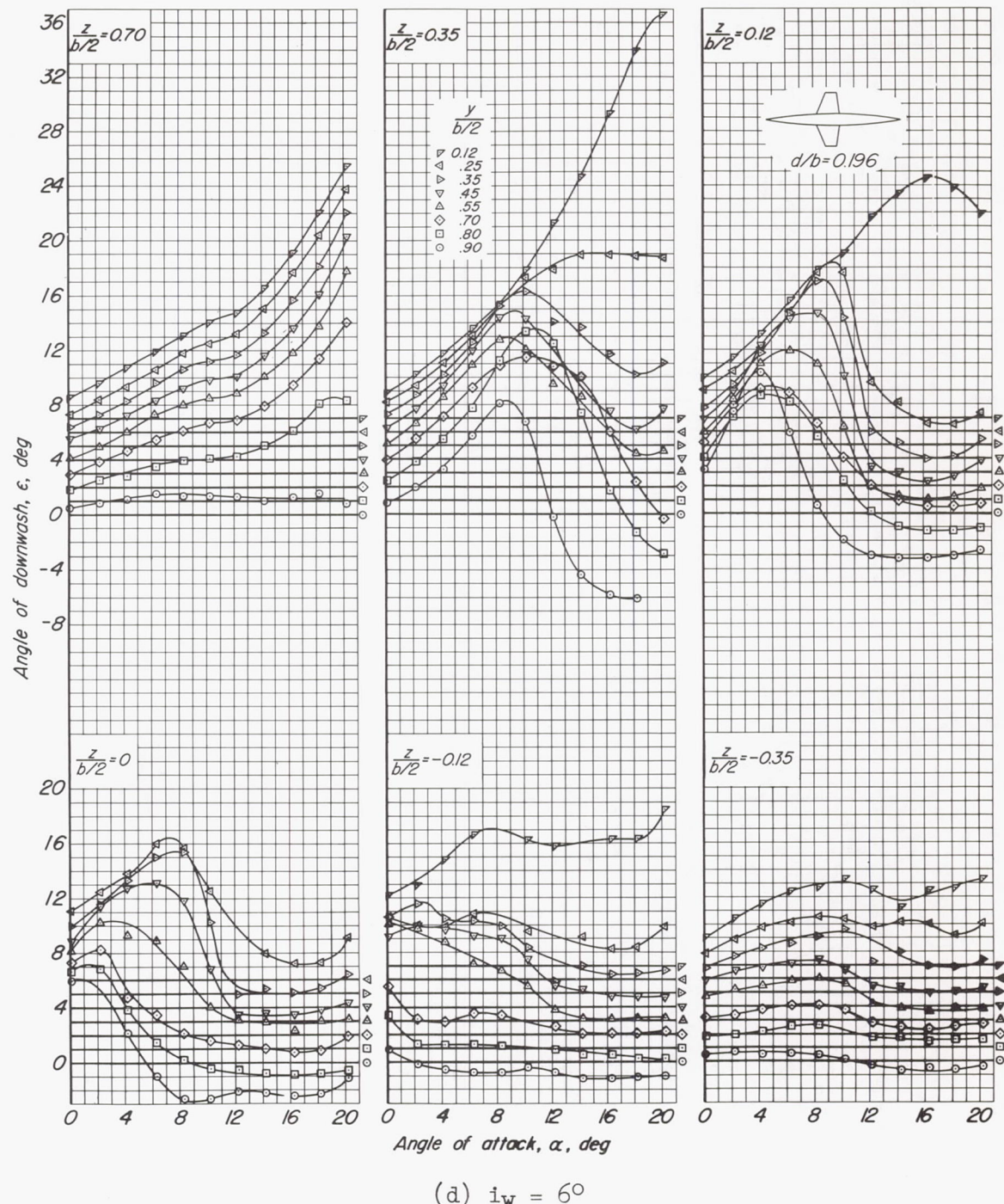


Figure 8.- Continued.

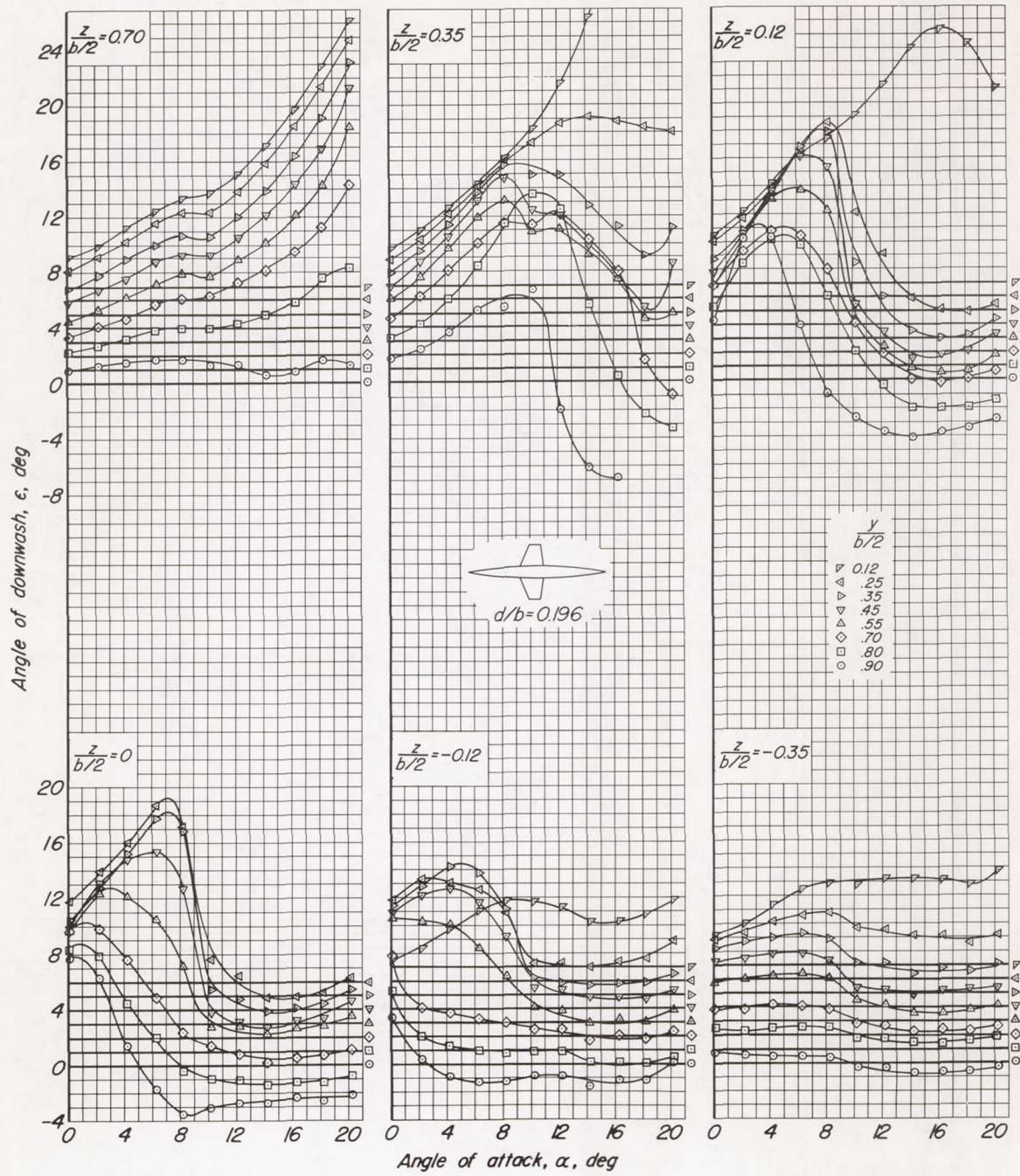
(e)  $i_w = 8^\circ$ 

Figure 8.- Continued.

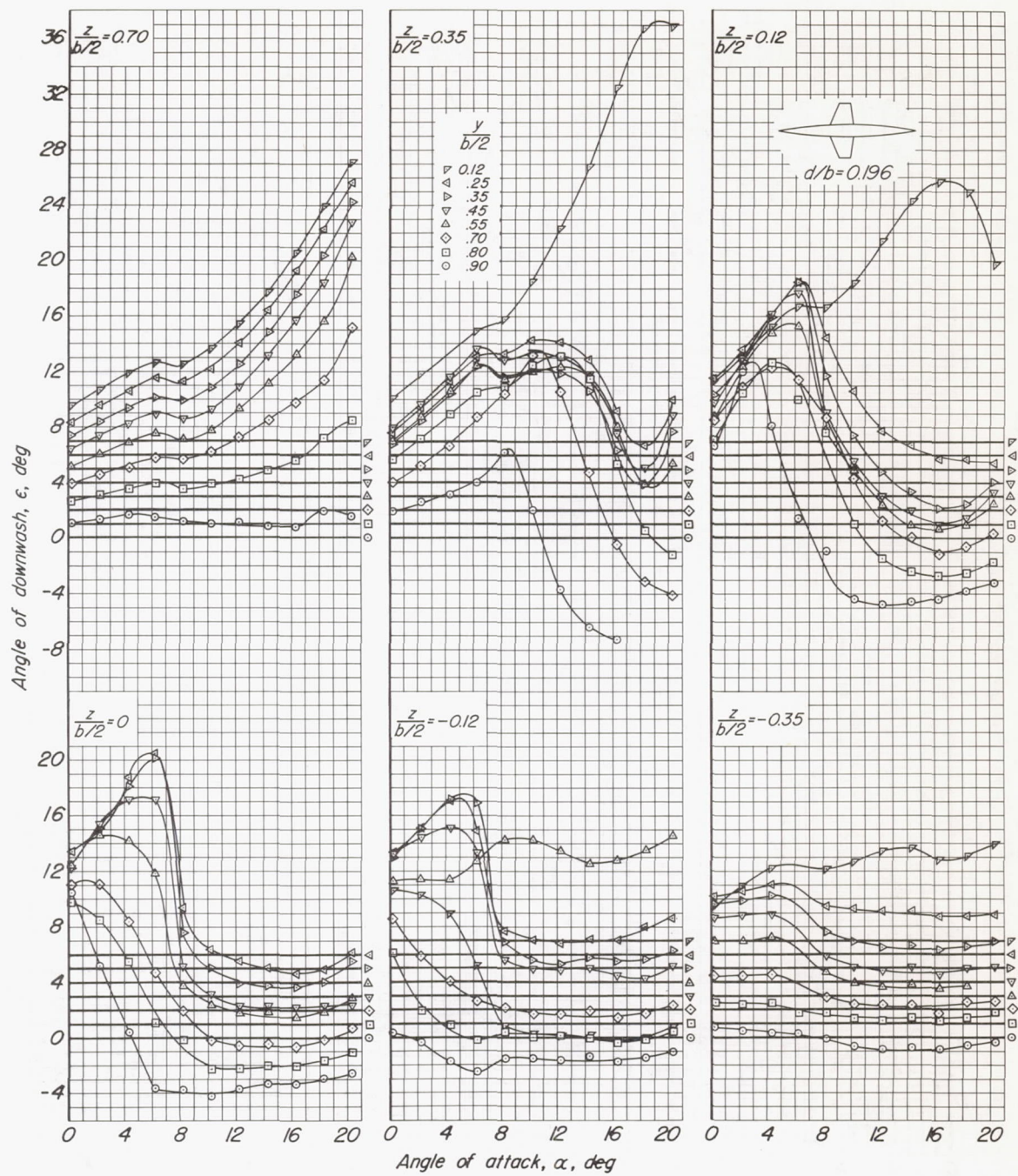
(f)  $i_w = 10^\circ$ 

Figure 8.- Concluded.

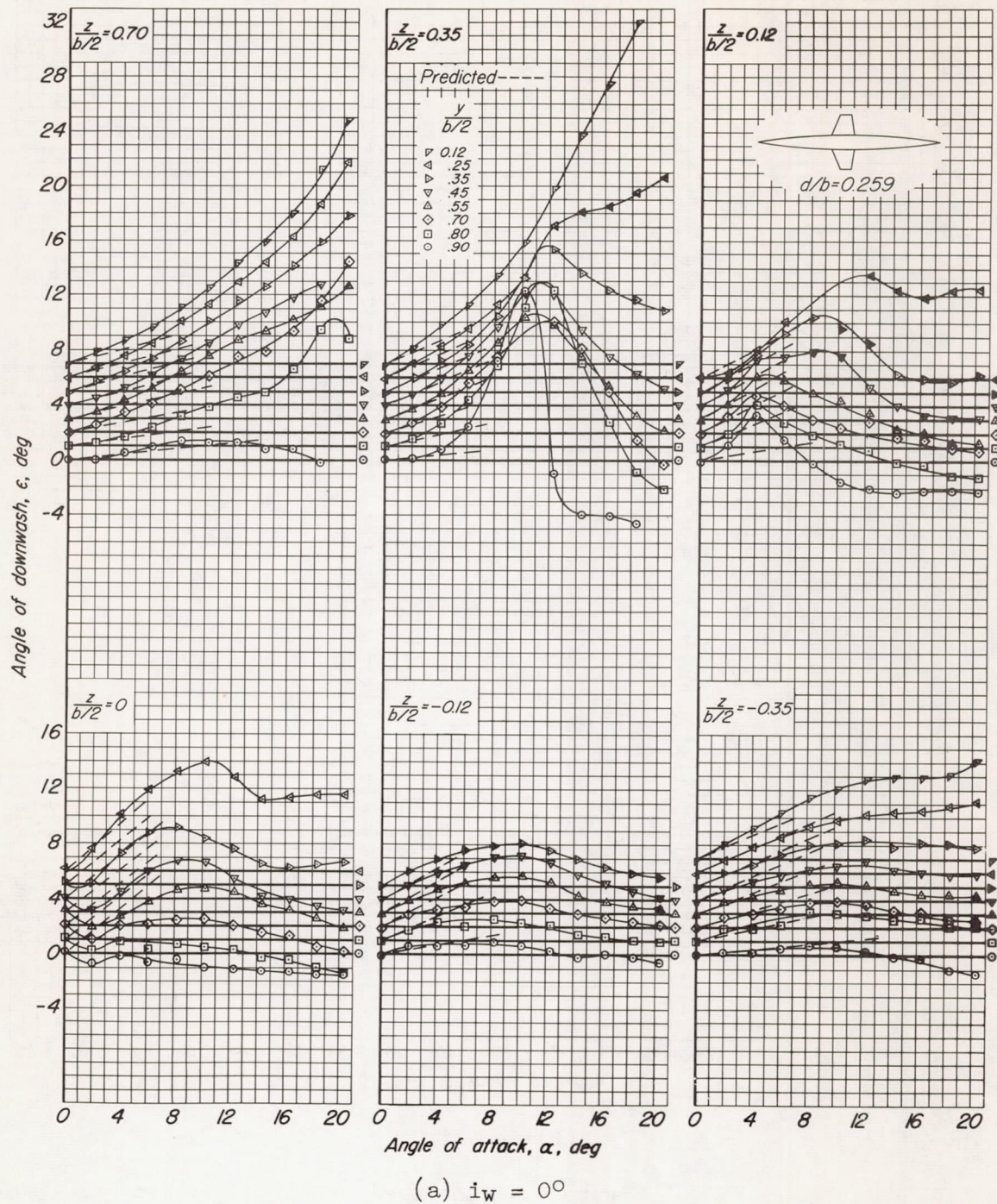


Figure 9.- Downwash in a plane  $2.31\bar{c}$  behind the  $0.25\bar{c}$  line of the trapezoidal wing of the wing-body combination having a ratio of maximum body diameter to wing span of 0.259.

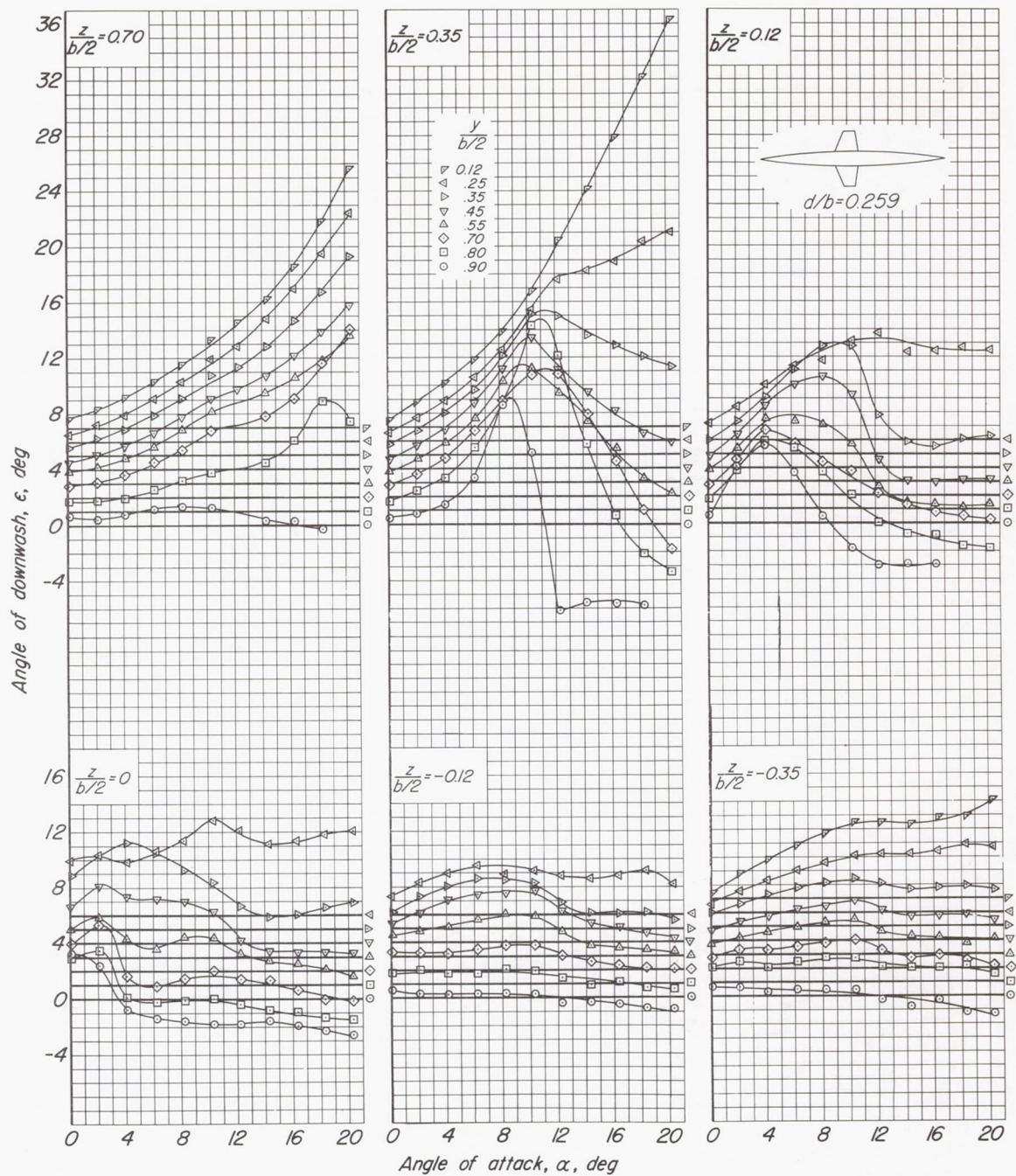
(b)  $i_w = 2^\circ$ 

Figure 9.- Continued.

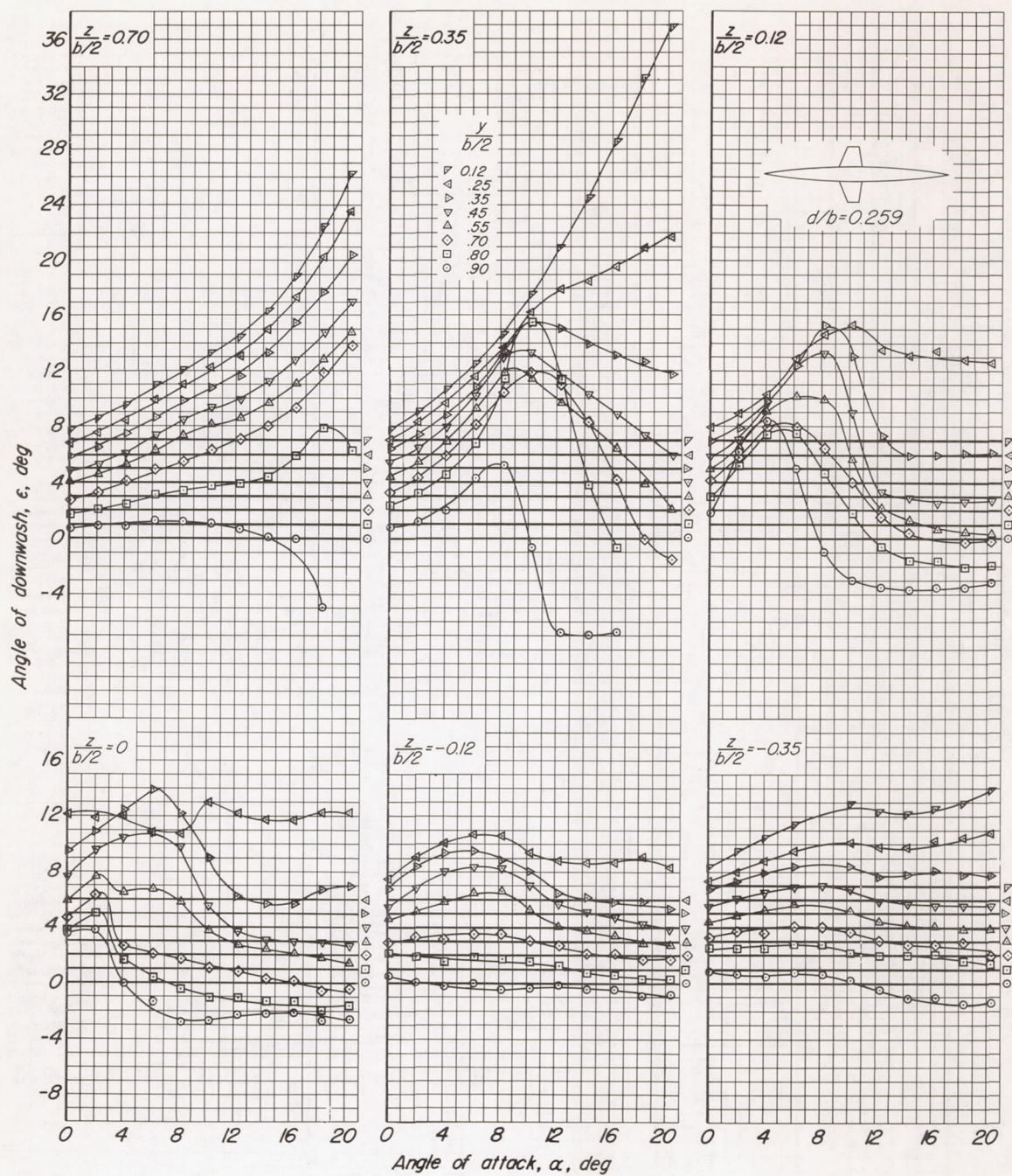
(c)  $i_w = 40^\circ$ 

Figure 9.- Continued.

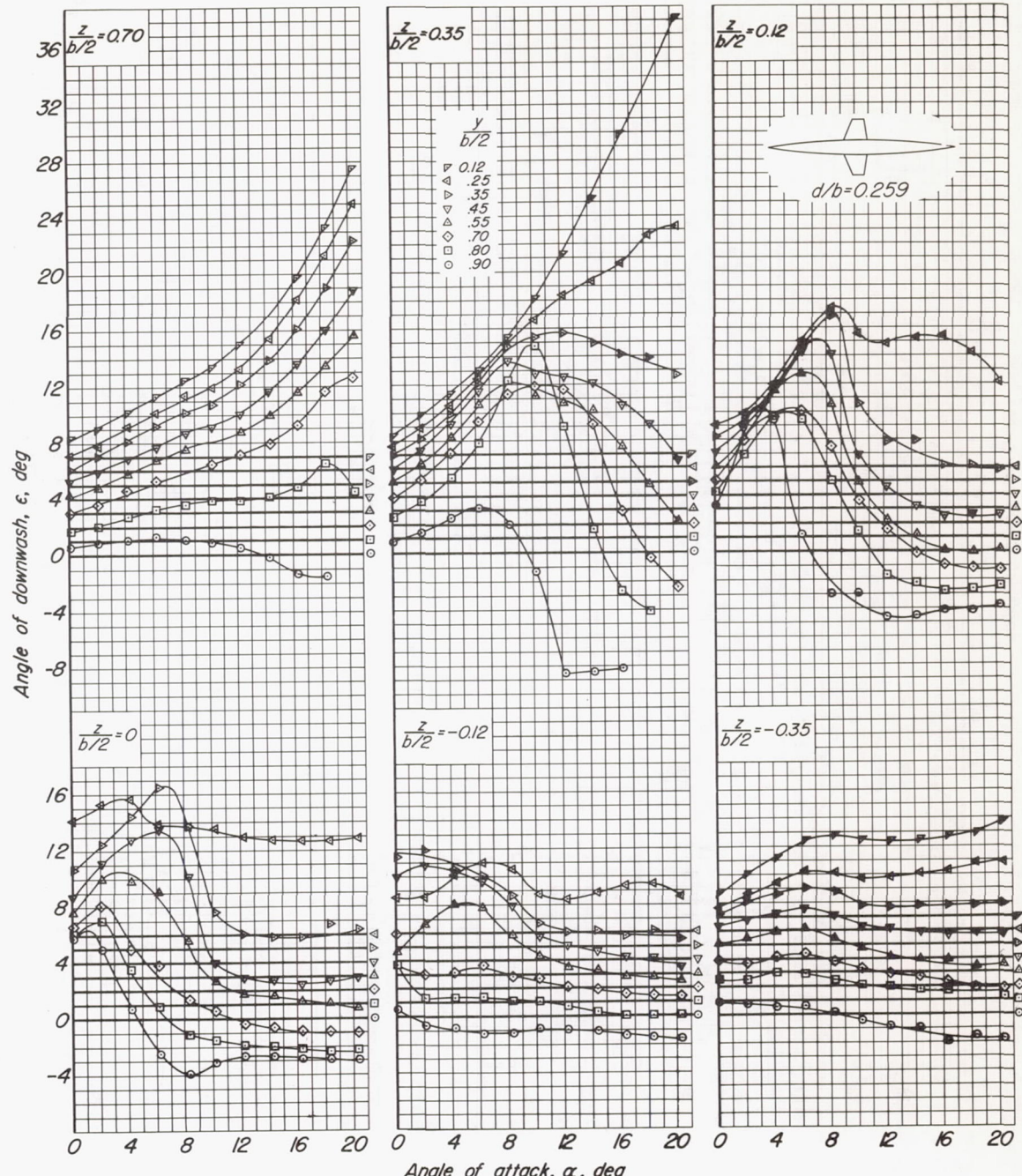
(d)  $i_w = 60^\circ$ 

Figure 9.- Continued.

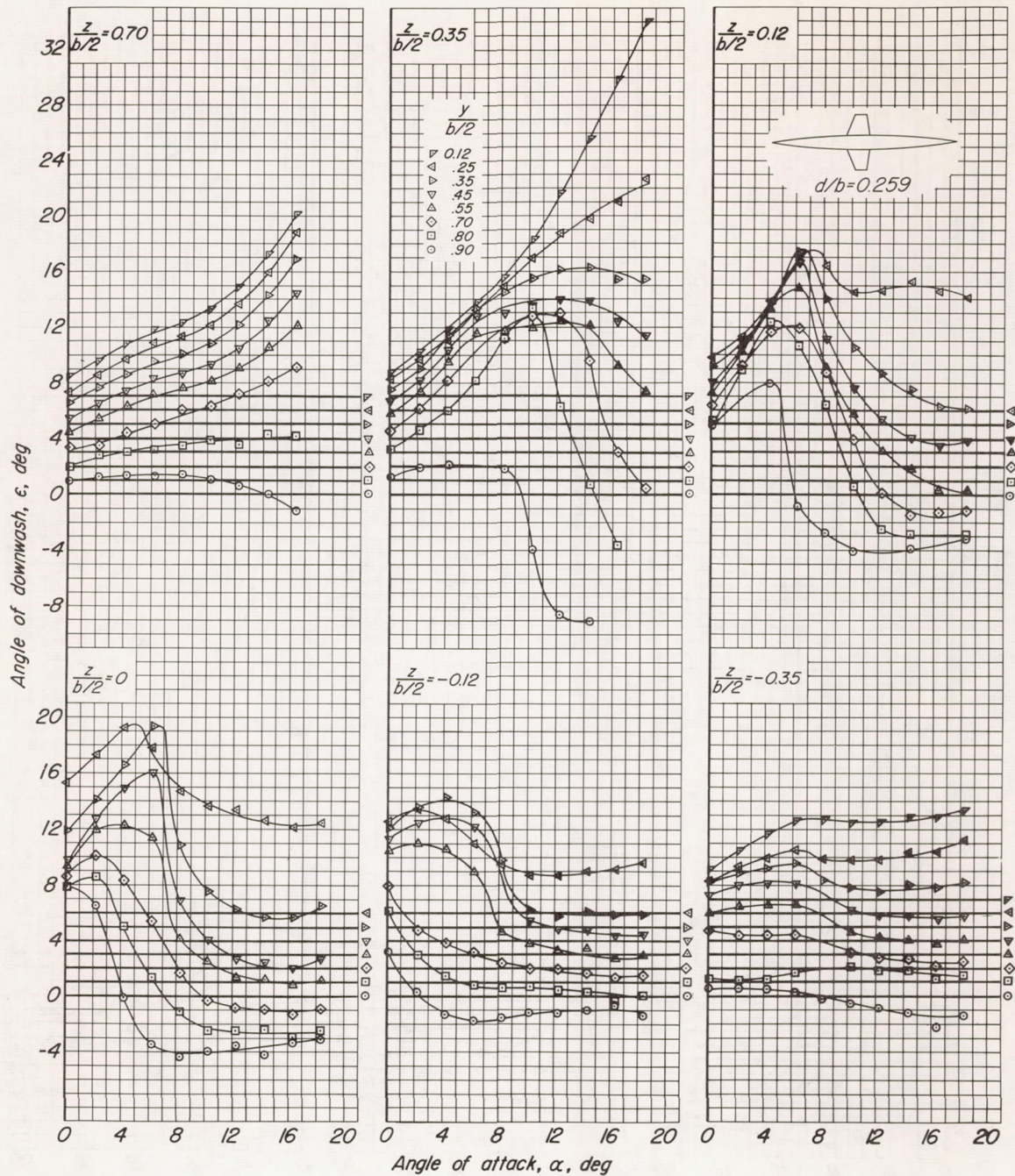
(e)  $i_w = 8^\circ$ 

Figure 9.- Continued.

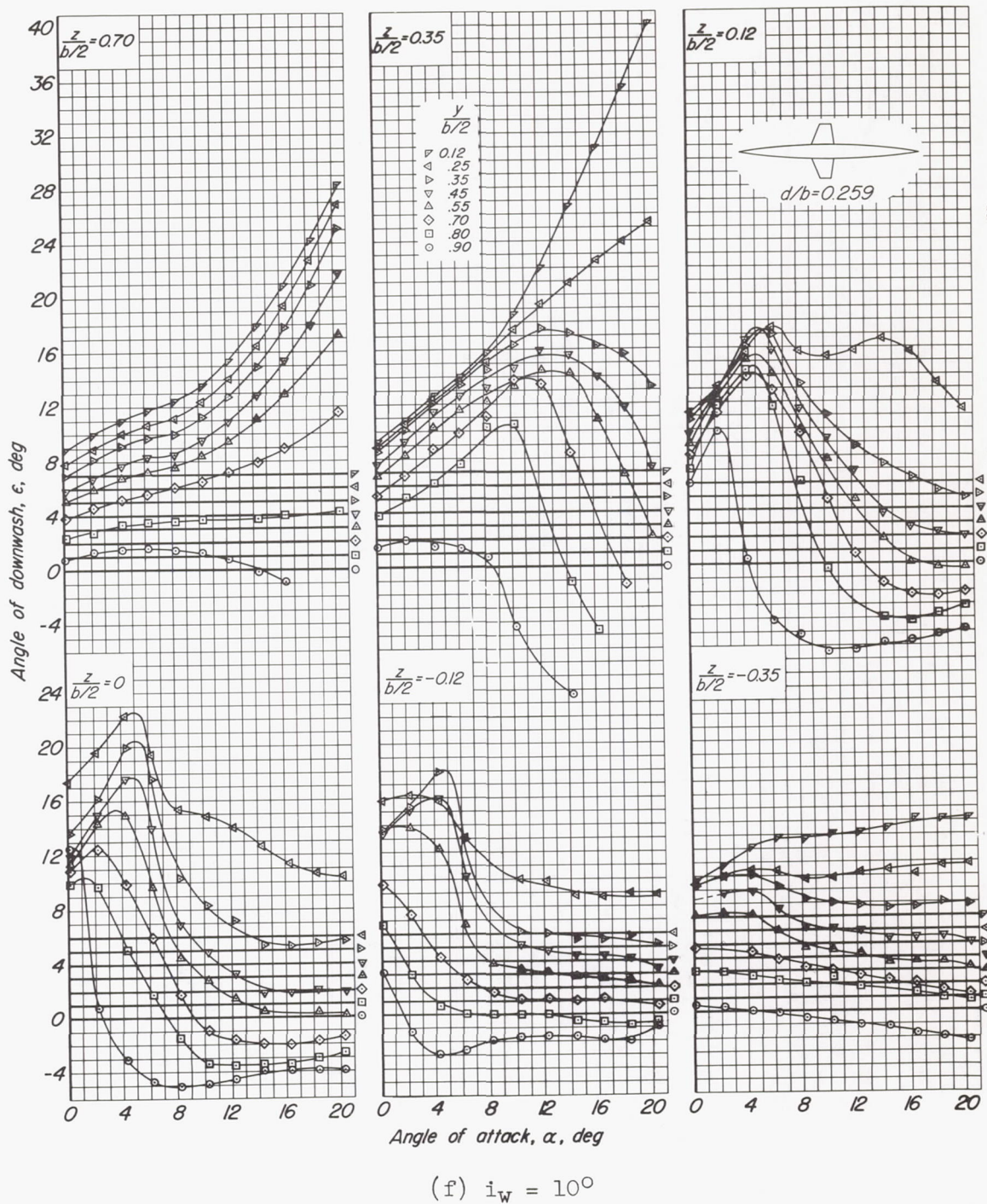


Figure 9.- Concluded.

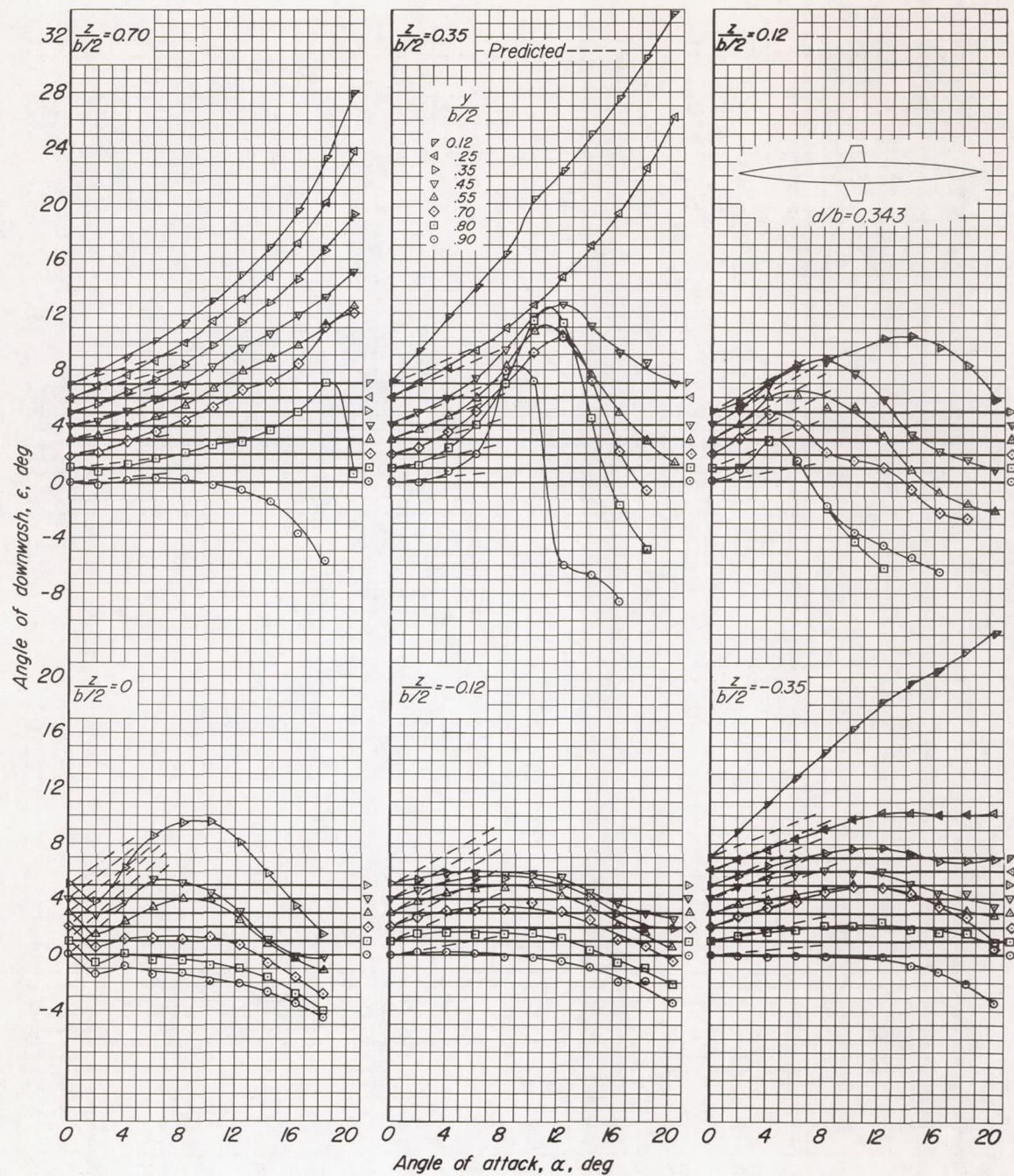
(a)  $i_w = 0^\circ$ 

Figure 10.- Downwash in a plane  $2.31c$  behind the  $0.25c$  line of the trapezoidal wing of the wing-body combination having a ratio of maximum body diameter to wing span of  $0.343$ .

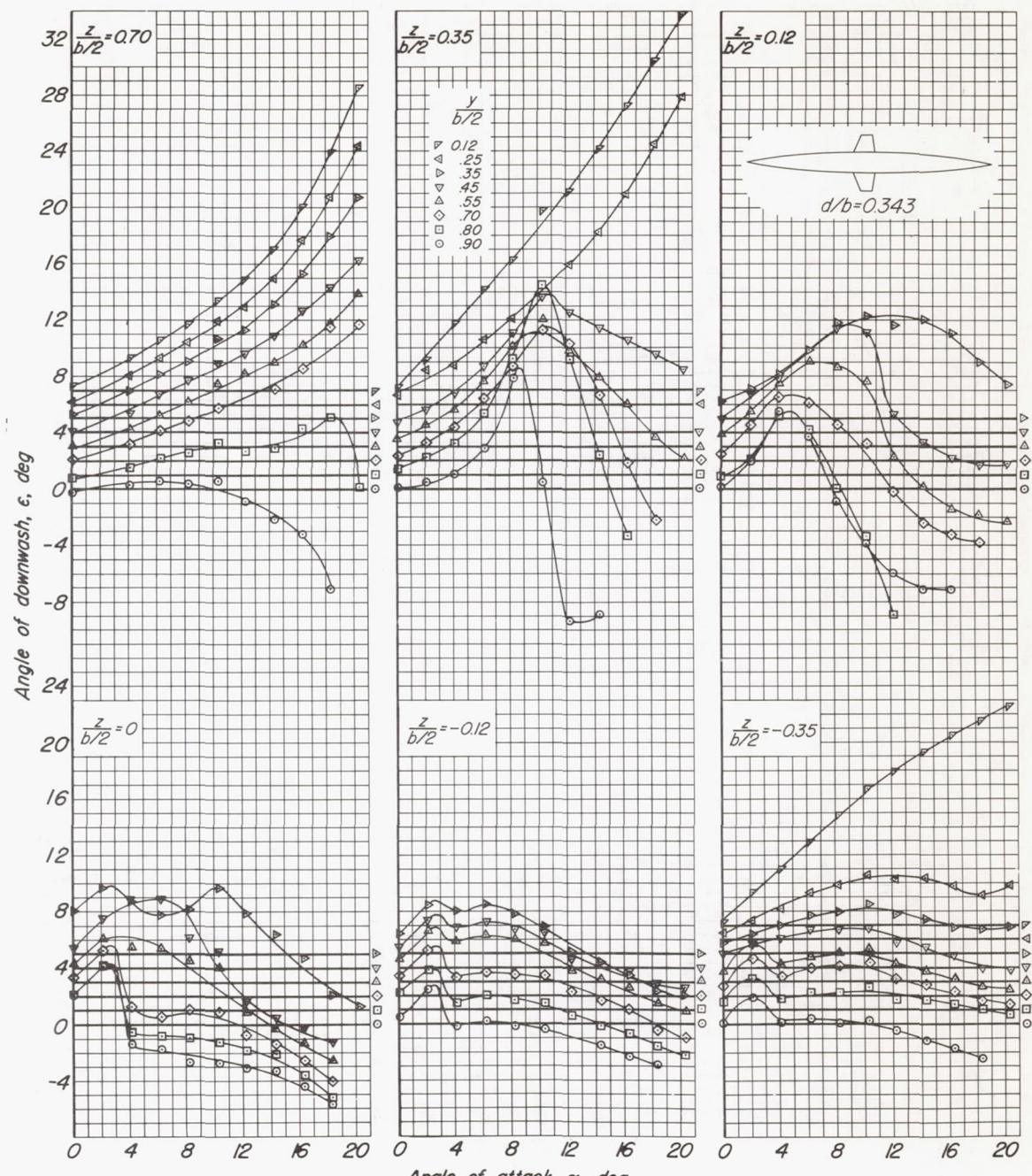
(b)  $i_w = 2^\circ$ 

Figure 10.- Continued.

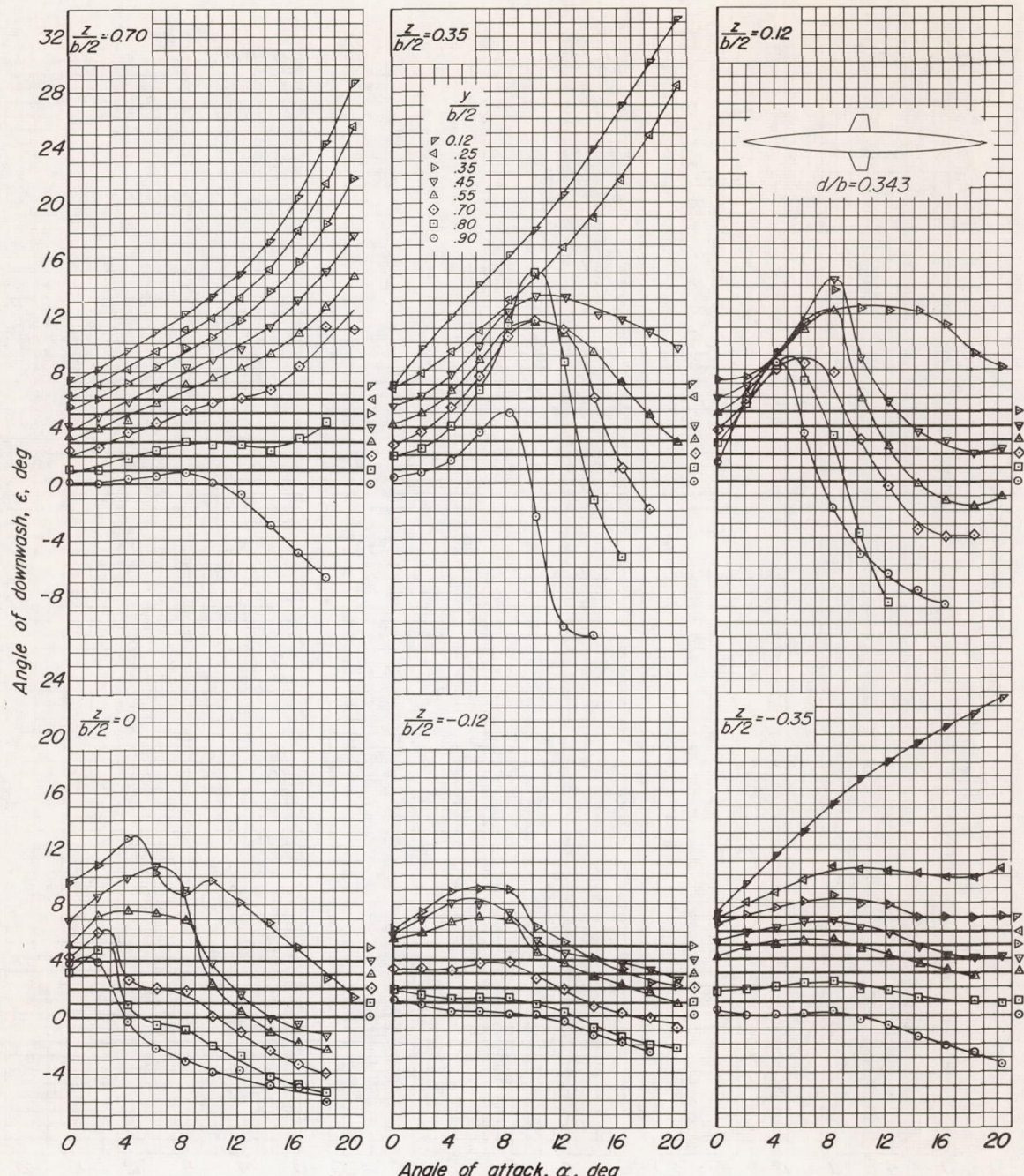
(c)  $i_w = 4^\circ$ 

Figure 10.- Continued.

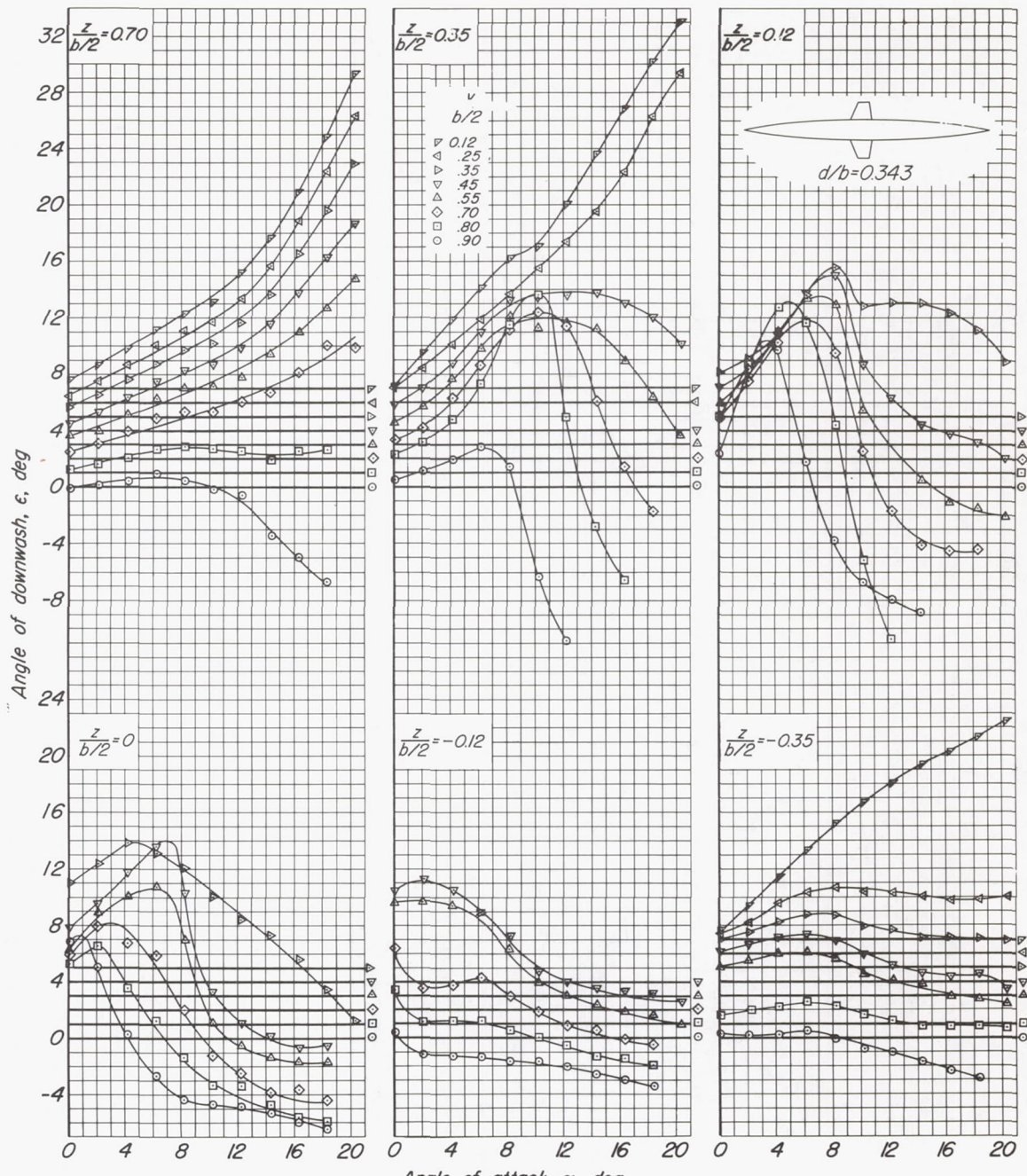
(d)  $i_W = 6^\circ$ 

Figure 10.- Continued.

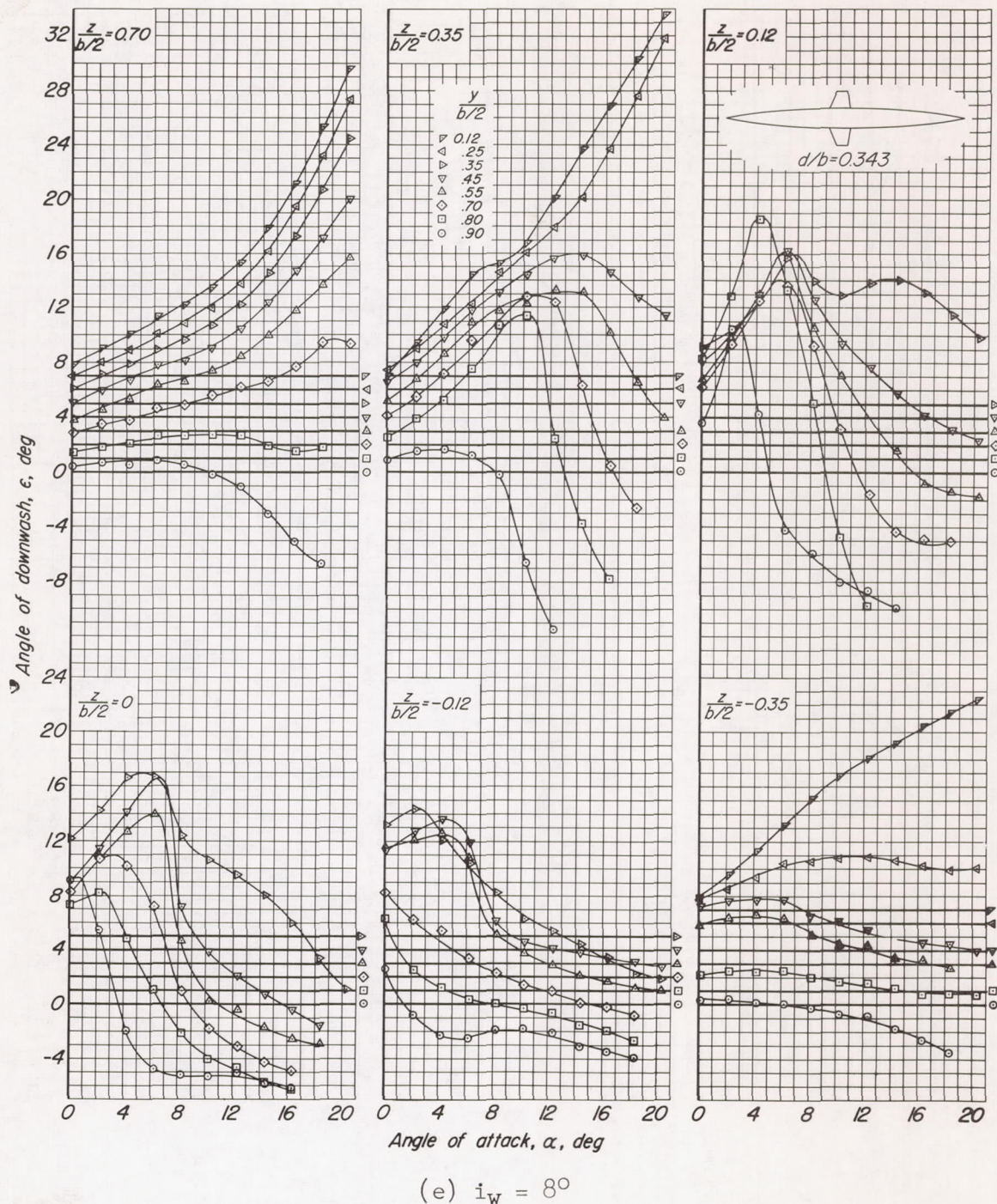
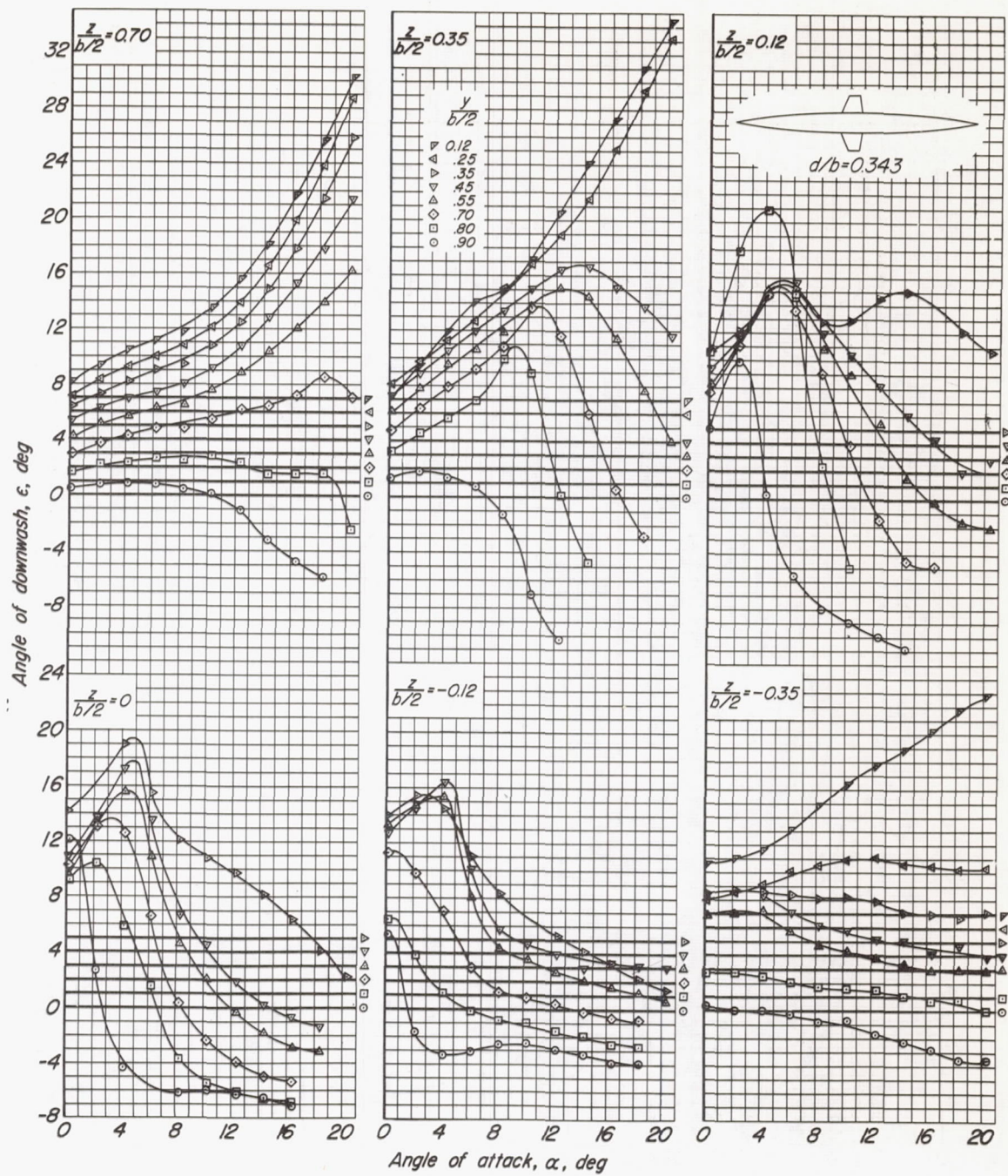


Figure 10.- Continued.



(f)  $i_w = 10^\circ$

Figure 10.- Concluded.